https://doi.org/10.5194/egusphere-2026-6814
Preprint. Discussion started: 12 November 2026
© Author(s) 2026. CC BY 4.0 License.

Characterization of atmospheric carbon at a remote high-alpine site

Leïla Simon[1,*], Nora Nowak[1,*], Stephen J. Andrews[2,3], Michael Bauer[1,a], David M. Bell[1], Benjamin T. Brem[1], Fabrizia Cavalli[8], Rico K.Y. Cheung[1,b], Zachary C.J. Decker[1,c,d], Jim R. Hopkins[2,3], Christoph Hüglin[7], Matic Ivančič[4], Alejandro Keller[5], Gašper Lavrič[4], Thierry Léonardis[6], Robin Modini[1], Jean-Philippe Putaud[8], Stefan Reimann[7], Martin Rigler[4], Thérèse Salameh[6], Martin Steinbacher[7], Martin K. Vollmer[7], Ernest Weingartner[5], Martin Gysel-Beer[1]

[1]PSI Center for Energy and Environmental Sciences, Villigen PSI, 5232, Switzerland
[2]Wolfson Atmospheric Chemistry Laboratories, The University of York, York YO10 5DD, United Kingdom
[3]National Centre for Atmospheric Science, The University of York, York YO10 5DD, United Kingdom
[4]Aerosol Magee Scientific, Kamniška 39A, Ljubljana, 1000, Slovenia
[5]Institute for Sensors and Electronics, University of Applied Sciences Northwestern Switzerland, Windisch, 5210, Switzerland
[6]IMT Nord Europe, Institut Mines-Télécom, Université Lille, Centre for Energy and Environment, Lille, 59000, France
[7]Laboratory for Air Pollution/Environmental Technology, Empa, Dübendorf, 8600, Switzerland
[8]European Commission, Joint Research Centre (JRC), Ispra, 21027, Italy
[a]now at: Aerosol Chemistry Department, Max Planck Institute for Chemistry, 55128 Mainz, Germany
[b]now at: Department of Environmental Sciences, University of Basel, Basel, 4056, Switzerland
[c]now at: Environmental Defense Fund, Boulder, CO, 80302, USA
[d]now at: Cooperative Institute for Research in Environmental Sciences, University of Colorado Boulder, Boulder, CO 80309, USA
[*]These authors contributed equally to this work

Correspondence to: Leïla Simon (leila.simon@psi.ch) and Martin Gysel-Beer (martin.gysel@psi.ch)

Abstract.

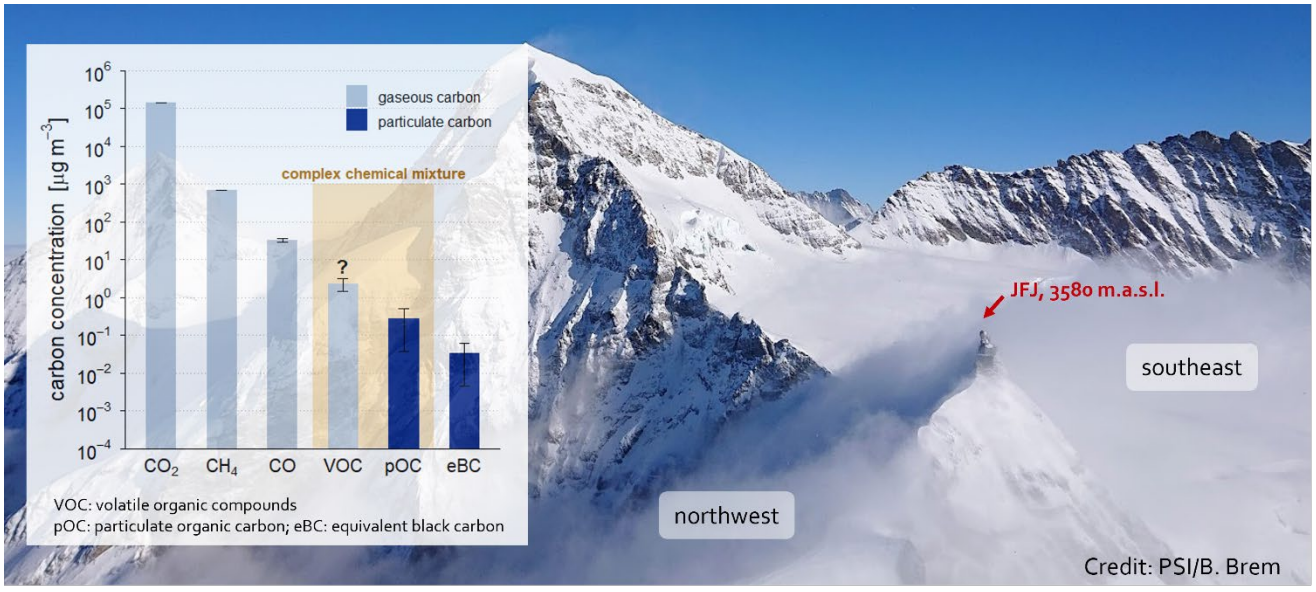
Carbon closure and volatility studies are needed to better constrain atmospheric carbon, but are especially lacking in high altitude sites, as these environments can be challenging to access. During a measurement campaign from 16 August to 20 September 2022 at Jungfraujoch (3580 m.asl, Switzerland), gas- and particle phase carbon was characterized using a broad suite of instruments, including a thermo-denuder upstream of a time-of-flight aerosol chemical speciation monitor to investigate particulate organic carbon (pOC) volatility. As expected in summer, the Jungfraujoch was mainly under planetary boundary layer influence (PBLi), with some periods in the free troposphere (FT). Moreover, a Saharan dust event and two wildfire plumes were identified.

The composition of fine particles was dominated by organic aerosol mass for all conditions, and particulate carbon measurements by different techniques captured similar temporal variability but showed systematic differences in absolute concentrations, especially at low concentrations. pOC was dominated by semi-volatile organic carbon, and a substantial part of OC could partition between gas and particle phase depending on pOC concentration and ambient conditions. PBLi conditions, compared to FT, showed higher concentrations of both gas and particle phase compounds, higher contribution of short-lived VOCs and higher pOC volatility. In addition, the wildfires affected OC concentrations and composition and

https://doi.org/10.5194/egusphere-2026-6814
Preprint. Discussion started: 12 November 2026
© Author(s) 2026. CC BY 4.0 License.

exhibited higher pOC oxidation state and lower inferred pOC volatility, coinciding with high m/z organic fragment signals. These findings contribute to a better understanding of the impacts of local and regional sources, and long-range transported plumes on free tropospheric carbonaceous compounds' concentrations and properties.

Graphical abstract:



1 Introduction

Carbon is present in the atmosphere under various forms and oxidation states, spanning from greenhouse gases such as carbon dioxide (CO_2), and methane (CH_4) to reactive gases like CO and to non-methane volatile organic compounds (VOCs) to particulate organic carbon (pOC) and black carbon (BC). Depending on the state of the carbon, it can have different impacts on both atmospheric chemistry and climate. Atmospheric concentrations of long-lived greenhouse gases such as CO_2 and CH_4 have increased substantially since pre-industrial times, modifying the Earth's radiation balance and driving global warming. In contrast, short-lived gaseous species and aerosols also perturb the Earth's radiative balance, but on much shorter time scales. Volatile organic compounds can oxidize in the presence of nitrogen oxides (NO_X) and lead to formation of secondary organic aerosol as well as tropospheric ozone (O_3), which is another greenhouse gas. SOA makes a substantial contribution to aerosol light scattering, which can mask greenhouse gas driven global warming. BC is the dominant atmospheric absorber of incoming solar radiation, and light-absorbing constituents of pOC can further contribute to this, thus causing dynamic feedbacks and affecting precipitation (Samset, 2022). Finally, carbonaceous aerosol has indirect effects, notably by impacting cloud formation and properties. In addition to its direct atmospheric warming effect through solar radiation absorption, BC can also accelerate the melting of snow and ice when deposited on bright surfaces. By reducing surface albedo, deposited BC increases solar

https://doi.org/10.5194/egusphere-2026-6814
Preprint. Discussion started: 12 November 2026
© Author(s) 2026. CC BY 4.0 License.

energy absorption, leading to enhanced warming and melt rates, particularly in glacier and polar environments (Bond et al., 2013).

While inorganic compounds such as CO, CO_2 and BC can generally be quantified and characterized more readily, atmospheric organic compounds comprise a far more complex chemical mixture. Depending on their volatility, ambient temperature, relative humidity, and the composition and abundance of condensed aerosol-phase material, organic compounds partition between the gas and particle phases. Reactive organic carbon also plays a role in atmospheric oxidative capacity. Upon atmospheric aging, the complex mixture of organic species in the atmosphere evolves and thereby its overall volatility changes. Often, organic compounds become more oxidized when they age, leading to lower volatility. Lower volatility organic compounds can condense and form secondary organic aerosol (SOA), which impacts air quality by reducing visibility and increasing health risks. However, fragmentation upon chemical reaction is an aging pathway that can increase the volatility of the species (Kroll et al., 2009). To better understand SOA formation and aging, studies with comprehensive characterization of gaseous and particulate carbonaceous species including volatility measurements are needed under various conditions. Isaacman-VanWertz et al. (2018, 2017) attempted such a characterization in an experimental chamber and were able to achieve full carbon closure with measurements of volatility, oxidation state and reactivity of the oxidation products of α-pinene precursor gas. The feasibility of such studies, however, depends on the availability of complex instrumentation that spans the full range of volatility from small, volatile gas compounds to refractory particles. This limitation makes it harder to bring carbon closure studies to the field, and indeed such studies are very scarce (Hunter et al., 2017; Yang and Fleming, 2019). Nonetheless, Hunter et al. (2017) were able to characterize and quantify atmospheric carbon in terms of carbon oxidation state versus volatility. This relationship is described in the two-dimensional volatility basis set (2D-VBS) introduced by Donahue et al. (2011), where the volatility is expressed as effective saturation mass concentration (C^*), which depends on saturation vapor pressure, at a specific temperature. The ambient concentration of OA will determine the fraction of a gaseous species partitioning into the particle phase, based on its own C^* value (Donahue et al., 2012). To improve modelling of global OC and better constrain its impacts, more measurements of carbon closure and volatility distributions are therefore needed, especially in understudied environments like the free troposphere (FT), where highly aged, long-range transported aerosols can be measured, which potentially reflect changes in the global air pollution. Moreover, little is known about how the planetary boundary layer (PBL) intrusions and the PBL-FT exchanges impact the carbon concentration and state in the FT and thus the potential local and global impacts. Aerosol mass closure between gravimetric measurements for total mass and the sum of inorganic ions measured by ion chromatography and total carbon measured by thermal analysis was achieved in the free troposphere, at Puy de Dôme in winter (Sellegri et al., 2003). This study was based on filters rather than online measurements, which does not allow for the assessment of sub-daily temporal variability.

The Jungfraujoch (JFJ) high altitude research station, located in Switzerland at 3580 m a.s.l., is part of the Swiss National Air Pollution Monitoring Network (NABEL), the Global Atmosphere Watch Programme (GAW), the Aerosol, Clouds, and Trace gases Research InfraStructure (ACTRIS) the Advanced Atmospheric Gases Experiment (AGAGE), and the Integrated Carbon

https://doi.org/10.5194/egusphere-2026-6814
Preprint. Discussion started: 12 November 2026
© Author(s) 2026. CC BY 4.0 License.

Observation System Research Infrastructure (ICOS) within which aerosol and trace gases have been measured continuously for several decades (Bukowiecki et al., 2016; Heiskanen et al., 2022; Hueglin et al., 2024; Mohr and Gysel-Beer, 2024; Prinn et al., 2018). In the context discussed here, these measurements provide insights on aerosol characteristics in the free troposphere and the impacts of aerosol sources on its concentration and properties. Early studies reported $PM_{2.5}$ concentrations of 3.76 µg m^{-3} on average during a summer month, with its composition dominated by organic substances (Krivácsy et al., 2001). Seasonal differences were observed in the particle number concentration and size distribution, illustrating the role of boundary layer injections in summer compared to clean free tropospheric conditions in winter (Weingartner et al., 1999). Building on this, longer-term PM_1 and coarse mode measurements highlighted a clear seasonality for all major components with lower concentrations in winter and higher concentrations in summer (Cozic et al., 2008). A 14-year climatology linking aerosol optical properties and weather types further refined this picture, showing the influence of both season and synoptic regime on boundary layer influence at JFJ, with the site being completely influenced by FT in winter during advective weather, and most PBL influenced in summer (including at night) during subsidence weather type (Collaud Coen et al., 2011). In a more recent study, the wintertime free tropospheric PM_1 concentrations were found to be very low (around 0.3 µg m^{-3} on average, Fröhlich et al., 2015) and reflected global background levels. This aerosol was generally highly aged due to distant sources, with oxygenated organic aerosol (OA) dominating the OA composition (Fröhlich et al., 2015), and composed mostly of small particles (<90 nm in diameter; Herrmann et al., 2015). On the other hand, PBL transport was shown to increase organics, nitrate and BC concentrations, to bring fresh organic aerosol (HOA) and to promote new particle formation and CCN concentrations (Fröhlich et al., 2015; Herrmann et al., 2015; Tröstl et al., 2016). In addition to planetary boundary layer intrusions, specific air masses can bring higher aerosol loadings, such as Saharan dust events (SDE; Collaud Coen et al., 2004, 2026) and wildfire plumes. With 625 000 visitors at the Jungfraujoch in 2022 (Jungfraubahn Holding AG, 2022), an additional source of reactive gases and aerosol is the local touristic activities, notably the restaurant, helicopters and cigarette smoke, which are generally flagged out of the aerosol measurements reported to ACTRIS/GAW (Bukowiecki et al., 2016; Fröhlich et al., 2015). For the gas phase, non-methane hydrocarbons (NMHC) and chlorinated organic compounds have been measured at JFJ using gas chromatography mass spectrometry since 2000. Lanz et al. (2009) applied positive matrix factorization (PMF) to 7 NMHC and 3 chlorinated compounds, which resolved 4 factors. NMHCs were mainly apportioned to 2 factors, one associated with aged combustion/natural gas and the other with fresh emissions/solvent use; while chlorinated compounds were associated with industrial VOC sources. The factors representing aged combustion/natural gas contributed the most (42%) and increased for air masses coming from Eastern Europe, Benelux, Southern Italy and England. Furthermore, oxygenated volatile organic compounds (OVOC) and NMHC were measured in 2005, with acetone (622-867 ppt), methanol (362-790 ppt), formaldehyde (303-505 ppt) and acetaldehyde (310-392 ppt) contributing 95% of the measured compounds in summer and 83% in winter (Legreid et al., 2008). However, studies linking particulate and gaseous carbonaceous compounds are lacking at this site.

https://doi.org/10.5194/egusphere-2026-6814
Preprint. Discussion started: 12 November 2026
© Author(s) 2026. CC BY 4.0 License.

The aim of this study is to characterize atmospheric carbon in both gas and particulate phase at the remote site of Jungfraujoch. For this, an intensive measurement campaign took place in late summer 2022 in the framework of ACTRIS-IMP project (Grant agreement ID: 871115), to observe both FT and PBL conditions. The ACTRIS/GAW measurements were complemented with state-of-the art instrumentation to measure both gaseous and particulate carbonaceous species. The research questions that this paper aims at answering are:

- Can we explain and quantify the various components of atmospheric carbon at a station that is frequently under clean free tropospheric influence?
- How do the different air masses and sources of gases and particles impact the observed levels and properties of carbonaceous species at this site?
- What is the volatility distribution of carbonaceous aerosol in the free troposphere? Is there a substantial portion of atmospheric carbon in the semi-volatile range for which partitioning between gas and particle phases is sensitive to total liquid aerosol concentration?

2 Methods

2.1 Measurement site

The campaign was carried out at the Jungfraujoch observatory from 16.8.2022 to 20.9.2022. This site is located in Switzerland at 3580 m. a.s.l. (46°32'N 7°59'E). The meteorological conditions at JFJ during the campaign are presented in Fig. S1 (Appenzeller et al., 2008). The temperature fluctuated around 0°C, except for a colder period in mid-September, when it fell below -10°C. A series of campaign-specific measurements were set up to complement the continuous monitoring activities described above. All aerosol instruments besides the High Volume (HiVol) filters for gravimetric PM_{10} determination and off-line chemical analysis sampled from a trace-heated whole-air inlet (World Meteorological Organization, 2016; Weingartner et al., 1999). All gas phase measurements, except for the Medusa-GC-MS, sampled from a common manifold. The HiVol sampler also sampled from this manifold. The 2020-Mönch inlet was used for the Medusa GC-MS measurements. The unheated inlet is located on the ridge towards the mountain Mönch and is connected to the instrument via 100 m heated inlet tubing (Sertoflex, 12 mm OD, 8.1 mm ID) (Vollmer et al., 2020). The inlet tubing used for the Medusa GC-MS measurements was flushed continuously (5 L min^{-1}) and an air sampling module allowed to branch off sample air to the instrument.

Table 1 summarizes the methods and instruments used in this study, most of which are online techniques, accompanied by daily HiVol 24h-filters for thermo-optical analysis downstream of a PM_{10} impactor. In addition, Fig. S2 shows the data coverage of all instruments.

https://doi.org/10.5194/egusphere-2026-6814
Preprint. Discussion started: 12 November 2026
© Author(s) 2026. CC BY 4.0 License.

Table 1: Instrumentation during the campaign, campaign-specific instruments are indicated in bold.

Phase	method or instrument	measured parameter
Particle	Condensation particle counter (CPC)	Particle number concentration (PNC) (Dp ≥ 10 nm)
	Mobility particle size spectrometer (MPSS)	Particle number size distribution (PNSD) 8.75 nm ≤ Dp ≤ 836 nm
	Fidas	Particle number size distribution (PNSD) ~300 nm ≤ Dp ≤ ~20 µm PM_1, $PM_{2.5}$ and PM_{10} mass concentration
	Total carbon analyzer (TCA)	Total carbon mass concentration
	Fast thermal carbon totalizator (FATCAT)	Total carbon mass concentration
	Aethalometer (AE33)	Aerosol light absorption
	Multi angle absorption photometer (MAAP)	Equivalent black carbon (eBC)
	Single particle soot photometer (SP2)	Refractory black carbon (rBC) mass concentration
	Integrating nephelometer	Aerosol light scattering
	Aerosol chemical speciation monitor (ACSM)	Non-refractory PM_1 mass concentration and chemical composition
	Thermo-denuder Scanning mobility particle sizer (TD-SMPS)	Aerosol volatility
	TD-ACSM	Aerosol volatility
	Thermo-optical analysis of filters	EC, OC (Eusaar)
Gas	Cavity ringdown spectroscopy	CO, CO_2, CH_4
	Gas chromatograph flame ionization detector mass spectrometer (GC-FID/MS)	C_2-C_{12} VOC, OVOC, BVOC
	Medusa GC-MS	C_2-C_7 VOC, halogenated trace gases
	GC-FID AirmoVOC	C_6-C_{20} VOC, mostly below LOQ
	Vocus proton-transfer reaction mass spectrometer (PTR-MS)	C_1-C_{24} VOC, with a proton affinity greater than that of water

https://doi.org/10.5194/egusphere-2026-6814
Preprint. Discussion started: 12 November 2026
© Author(s) 2026. CC BY 4.0 License.

2.2 Online aerosol measurements

2.2.1 Number concentration and size distribution

The total particle number concentration was recorded with a condensation particle counter (CPC) model 3772 (TSI, Shoreview, MN, USA) operating at a lower cut-off diameter of 7.5 nm. Simultaneously, the particle-size distribution in the 8.75–836 nm range was obtained using a mobility particle size spectrometer (MPSS) (Tropos, Germany). The MPSS system comprised a Kr-85 neutralizer, a Hauke-type medium-differential mobility analyzer (DMA) with an effective length of 28 cm, and a CEN-CPC model 3750 for downstream counting. The DMA operated at a DMA voltage of 0 to 7 kV and a sheath flow of 5 L min^{-1}, yielding the stated size range above at a time resolution of 5 min. Further technical specifications of the MPSS instruments, including measurement uncertainties and data-quality control procedures are described in detail by Wiedensohler et al. (2012). An additional custom SMPS instrument was further connected downstream of the TD. This instrument utilized a TSI Long DMA Model 3081 and a TSI CPC Model 3775 also in combination with a Kr-85 neutralizer allowing the sizing between 16 and 700 nm. It should be noted that to keep comparison with the ACSM that has a cut-off diameter around 700 nm, the MPSS data was not extrapolated to the range 700-1000 nm. PM_1 mass concentrations were obtained from number size distribution assuming spherical particles and with a density (ρ) calculated as:

$$\rho = \left(\frac{f_{Inorg.}}{1.75} + \frac{f_{Org.}}{1.27} + \frac{f_{eBC}}{1.8}\right)^{-1} \quad (1)$$

With $f_{Inorg.}$, f_{Org}, f_{eBC} the fraction of inorganic NR-PM_1 species (NO_3^- + SO_4^{2-} + NH_4^+ + Cl^-), organic aerosol and equivalent black carbon in PM_1 (calculated as their sum in this case), respectively. The average density in this work was 1.42 g cm^{-3}.

Coarse mode aerosol number concentrations and size distributions (0.18–18 µm optical diameter) were recorded with a PALAS FIDAS 200 white-light optical spectrometer, operating at 1 min resolution. Tightness and the inlet flow rate were regularly checked with a reference flow meter. The instrument's counting-efficiency and size-bias was frequently checked using the CalDust routine (Empa, 2025).

2.2.2 Total carbon concentration

Online total carbon measurements were performed with two total carbon (TC) analysers, the TCA 08 (Aerosol Magee Scientific, Slovenia; Rigler et al., 2020) and the fast thermal carbon totalizator (FATCAT, FHNW, Switzerland; Keller et al., 2023). Both instruments determine TC concentrations through a semi- continuous, two-step collect-and-analyse cycle. During the sampling step, ambient aerosol particles are collected on a filter over a user-defined time interval. In the subsequent analysis step, the filter is rapidly heated under an oxidizing atmosphere, thermally decomposing and combusting the carbonaceous material, which is then quantified as CO_2 by a non-dispersive infrared (NDIR) detector. Both instruments use an upstream honeycomb charcoal denuder (Aerosol Magee Scientific, Slovenia) to remove gas-phase OC which could be absorbed by the sampling filter causing positive measurement artifacts.

https://doi.org/10.5194/egusphere-2026-6814
Preprint. Discussion started: 12 November 2026
© Author(s) 2026. CC BY 4.0 License.

The two instruments differ in a few design aspects (see e.g., Corbin et al., 2024). The TCA08 collects aerosol on a 47 mm quartz-fibre filter, which is flash-heated, and features two parallel sampling channels that alternate between collection and analysis, enabling quasi-continuous operation without measurement gaps. The FATCAT, in contrast, collects aerosol on a sintered metallic filter, which uses homogeneous induction-based flash heating throughout the sampling-filter and produces reproducible thermograms which can provide qualitative information on the volatility and chemical composition. A downstream platinum catalytic converter, heated to 200°C, ensures complete oxidation of all carbonaceous gases to CO_2 before detection by the NDIR sensor.

The TCA08 operated at a sample flow of 16.7 L min^{-1}, which was calibrated on-site and set to JFJ conditions. In addition, an on-site, offline validation of the carbon constant was performed using calibration filters (ambient aerosols) previously verified by OC/EC analysis, and this on-site, offline validation was used to assess the influence of JFJ conditions on the analytic air (filtered ambient air) of 0.5 L min^{-1}. The upper cut-off of the instrument is 10 µm.

FATCAT was operated with a 2 h time resolution, producing one data point per measurement cycle. The sampling flow rates were continuously monitored and regulated by mass flow controllers (MFCs) calibrated at standard temperature and pressure (STP: 273.15 K, 1013.25 hPa). Consequently, all FATCAT concentration data were converted to local Jungfraujoch conditions by applying a scaling factor of 0.588, corresponding to a local reference temperature of 298.15 K and a pressure of 650 hPa. During each 2 h cycle, FATCAT sampled a volume of approximately 0.8 m^3_{STP} of ambient air. This relatively low sampling rate of ~7 L min^{-1} (compared to the ~10 L min^{-1} maximum flow rate of the instrument) is the result of the reduced atmospheric pressure at the high-alpine site in combination with the flow resistance of the sintered metallic filter. During analysis, the filter is heated inductively from ambient temperature to ~800 °C in less than 1 min; as this ramp is highly reproducible, the elapsed heating time serves as a proxy for the filter temperature (Keller et al., 2026, 2023). The instrument samples particles up to about 3 µm.

2.2.3 Optical properties, equivalent black carbon (eBC) and refractory black carbon (rBC)

Aerosol optical properties and eBC concentrations were obtained from the permanently installed long-term monitoring instrumentation on Jungfraujoch which include a three wavelength integrating nephelometer (Model 3563, TSI, USA), a single wavelength Multi-Angle Absorption Photometer (MAAP, Model 5012, Thermo Fisher Scientific, USA) and a seven wavelength aethalometer with internal loading compensation (Model AE-33, Aerosol Magee Scientific, Slovenia). The instruments were operated according to GAW 227 (World Meteorological Organization, 2016) and ACTRIS recommendations which included daily zero adjustments for the nephelometer and monthly zero checks for the MAAP and AE-33 instruments. A bimonthly CO_2 span calibration was performed on the nephelometer. The data processing adhered to the ACTRIS guidelines for each instrument. The total light scattering coefficients were corrected for truncation based on the Anderson and Ogren scheme recommended for this instrument (Anderson and Ogren, 1998). MAAP data were processed for the light absorption coefficient according to Müller et al. (2011). The loading compensated BC output of the AE-33 was used for deriving the AE-

https://doi.org/10.5194/egusphere-2026-6814
Preprint. Discussion started: 12 November 2026
© Author(s) 2026. CC BY 4.0 License.

33 absorption by using a H factor of 1.76. The conversion to eBC was performed on the MAAP using the ACTRIS-harmonized mass absorption cross-section (MAC) of 10 m^2 g^{-1} at the 637 nm wavelength (Favez et al, 2024; Zanatta et al., 2016).

A single particle soot photometer (SP2; Droplet Measurement Technologies; Schwarz et al., 2006) was used to measure refractory black carbon mass concentration (rBC), which refers to BC quantified by means of laser-induced incandescence (Petzold et al., 2013). The SP2 was calibrated using size-selected "fullerene soot" as detailed in Baumgardner et al. (2012), Gysel et al. (2011), and Laborde et al., 2012).

2.2.4 Aerosol mass spectrometry

Non-refractory PM_1 species were quantified by mass spectrometry as organic aerosol (OA), nitrate (NO_3^-), ammonium (NH_4^+), sulfate (SO_4^{2-}) and chloride (Cl^-). The ACTRIS monitoring time-of-flight aerosol chemical speciation monitor (ToF-ACSM, Aerodyne Inc., USA and Tofwerk, Switzerland) was complemented with a second ToF-ACSM for the volatility measurements (see below). Both ACSMs were equipped with a critical orifice of 120 µm instead of 100 µm due to the lower pressure at high altitude. The flow rate was calibrated at local conditions and was around 2.2 cm^3 s^{-1} (0.132 L min^{-1}) during the campaign. They were sampling at a time resolution of 40s and the mass spectra ranged from mass-to-charge ratio (*m/z*) 12 to 200. Note that while the ACSM has a PM_1 lens, its transmission efficiency decreases for particle below 70 nm and above 700 nm (vacuum aerodynamic diameter). For the ACTRIS ACSM, a first calibration was performed at the beginning of the campaign on 14.08.22 and a second one after the campaign on 03.10.2022 (see Ng et al. (2011) for details on the calibration procedure). The averaged parameters from both calibrations were used for the data treatment. For the second ACSM, a first calibration was done on 15.08.2022, a second one on 22.08.2022 after the filament emission was increased, and a last one on 03.10.2022. A CE of 1 was used in the data treatment, in agreement with previous studies with AMS or ACSM at JFJ (Fröhlich et al., 2013; Jurányi et al., 2010; Lanz et al., 2010) and validated by comparing the sum of NR-PM_1 from the ACSM and eBC from MAAP with PM_1 mass concentration obtained from volume concentration of the MPSS (Fig. S3c). Limits of detection (LOD) were calculated for the ACSM species, as well as for m/z 43 and m/z 44. Blank measurements were performed by placing a HEPA filter in front of the ACSM inlet overnight. The LOD were then calculated as 3 times the standard deviation of these measurements, on a 1-hour time resolution. They ranged from 1.26 ng m^{-3} for m/z 43 to 0.176 µg m^{-3} for OA from the ACSM used for volatility analysis (TD-ACSM).

Elemental ratios for the organic matter were calculated based on the ACSM mass spectrum (Canagaratna et al., 2015):

$$O{:}C = 0.079 + 4.31 * f44 \quad (2)$$

$$H{:}C = 1.12 + 6.74 * f43 - 17.77 * f43^2 \quad (3)$$

$$OA{:}OC = 1.29 * O{:}C + 1.17 \quad (4)$$

$$OSc = 2 * O{:}C - H{:}C \quad (5)$$

*f*43 is the fraction of mass concentration at *m/z* = 43 to total OA mass concentration, similarly *f*44 is the fraction of the mass concentration at *m/z* = 44 to total OA mass concentration. OSc is the average oxidation state.

https://doi.org/10.5194/egusphere-2026-6814
Preprint. Discussion started: 12 November 2026
© Author(s) 2026. CC BY 4.0 License.

2.2.5 Volatility

Aerosol volatility measurements were done by placing a thermodenuder (TD) upstream of both an ACSM and an SMPS instrument (Fig. S4). The residence time in the TD was 4.5 seconds. The thermodenuder (Aerodyne) was then set to four temperatures (Table 2). The temperature setpoints were 50°C, 100°C, 150°C and 200°C and changed every 15-25 min. Every day, the TD was bypassed to compare the two ACSM against each other, and the monitoring ACSM was used to have a constant measurement of aerosol mass at 25°C to compare against.

Thermodenuder temperatures were mapped to approximate effective saturation mass concentration ($\log10_{eff}$ C^*) ranges using the mass-transfer model of Saha and Grieshop (2016), with the relationship between vaporization enthalpy and saturation concentration parameterized following Epstein et al. (2010). The simulated evaporation responses (Fig. S5) were used to define the broad volatility ranges in Table 2 at 298.15 K. These ranges are model-dependent estimates rather than direct measurements of C^*. The highest-volatility interval represents material lost between approximately 25 and 50 °C and was derived by combining measurements from the two ACSMs; it therefore carries additional inter-instrument uncertainty. The two lowest-volatility classes were combined into an ELVOC–NVOC category.

Table 2: Thermo-denuder temperatures and the respective $\log10_{eff}$ C^* and volatility classes of organic carbon at 298.15 K

TD-temperature	$\log10_{eff}$ C^*	Volatility class of organic carbon
150°C – 200°C	-17 to -10	Non volatile (NVOC) to extremely low volatile (ELVOC)
100°C – 150°C	-9 to -3	ELVOC to low volatile (LVOC)
50°C – 100°C	-3 to 1	LVOC to semi volatile (SVOC)
25°C – 50°C	1 to 3	SVOC

2.3 Offline aerosol measurements

2.3.1 Filter collection

Daily 24 h PM_{10} bulk aerosol samples were collected using a high-volume sampler (DHA-80, Digitel, Switzerland) operated at a sampling volume of approximately 1075 m^3 day^{-1}. The sampler was connected to a stainless-steel inlet (90 mm inner diameter, ~3 m length, inlet ~2 m above the roof) maintained at 10 °C, with a PM_{10} size-selective impactor installed directly upstream of the sampler. Particles were collected on quartz-fibre filters (Pallflex). The instrument was equipped with an automatic filter-changing system and a 15-filter magazine, allowing uninterrupted sampling and automatic filter exchange at midnight.

https://doi.org/10.5194/egusphere-2026-6814
Preprint. Discussion started: 12 November 2026
© Author(s) 2026. CC BY 4.0 License.

2.3.2 Gravimetry

The gravimetric determination of particulate matter (PM) mass concentration from quartz fibre filters complies with EN 12341. Prior to sampling, filters are pre-baked at 500°C to eliminate organic contaminants, then equilibrated for 96 hours in a climate-controlled room at 20 ± 1°C and 50 ± 5% relative humidity to record their tare weight using a high precision microbalance with antistatic-kit (XP205, Mettler Toledo, USA). After re-equilibrating the filters under identical temperature and humidity conditions for another 96 hours, the final gross mass is recorded. The net PM mass loading is calculated by subtracting the tare weight, adjusted using parallel field blanks to correct for passive artifacts, and normalized against the total standardized sampling volume to establish the ambient concentration in µg m^{-3}.

2.3.3 OC/EC concentrations by thermal optical analysis

Thermal-optical analysis (TOA) was performed to determine the organic carbon (OC) and elemental carbon (EC) content of the quartz fibre filters following the European standard protocol EN 16909. Aliquots of 1.5 cm^2 were taken from the conditioned filters and analyzed using a Sunset Laboratory Thermal-Optical Carbon Aerosol Analyzer. The analysis followed the standard EUSAAR_2 temperature protocol, which sequentially volatilizes OC in an inert helium atmosphere up to 650°C, followed by the combustion of EC in a helium/oxygen mixture up to 850°C. To accurately account for the pyrolytic conversion of OC to EC during the inert phase, continuous optical monitoring was conducted using a tuned diode laser to trace filter transmission. The split point between OC and EC was automatically defined when the laser signal returned to its initial pre-baked baseline, and the final carbon masses were blank-corrected and normalized against the sampled air volume to yield atmospheric concentrations in µg C m^{-3}.

2.4. Gas phase measurements

2.4.1 CO_2, CO and CH_4

Air for the continuous CO_2, CO, and CH_4 measurements was sampled from the main manifold upstream of the HiVol PM_{10} impactor. The sample air was transported to the analyser through a 10 m long Sertoflex tube (1/4″ OD) at a flow rate of 4 L min^{-1}. CO_2, CO, and CH_4 were quantified simultaneously using a high-precision wavelength-scanned cavity ring-down spectrometer (CRDS; G2401, Picarro Inc., USA) coupled to a custom-built calibration and sample-drying unit. Water vapour was removed using a Nafion dryer (PermaPure) to minimize H_2O-related spectral interference. As the instrument simultaneously measures trace levels of H_2O, the CO_2, CH_4, and CO mole fractions were further corrected during post-processing using an empirical humidity correction to account for any residual dilution and pressure-broadening effects. CO_2, CH_4, and CO are reported as dry-air mole fractions. The system underwent automated, regular calibrations (3 reference tanks, every 9 days) against pressurized reference air standard tanks traceable to the World Meteorological Organization (WMO) scale. Two target tanks, treated as unknowns, were measured daily and two-weekly, respectively, as additional quality assurance to control for short-term and longer-term inconsistencies in the observations and/or the post-processing.

https://doi.org/10.5194/egusphere-2026-6814
Preprint. Discussion started: 12 November 2026
© Author(s) 2026. CC BY 4.0 License.

2.4.2 Gas chromatography

NMHCs and oxygenated VOCs were measured with a gas chromatograph–flame ionization detector/mass spectrometer (GC–FID/MS). Air was drawn from the shared manifold down ¼" Silonite (Entech) coated heated stainless steel tube at 20-30 slpm using a metal bellows compressor pump (Senior Aerospace MB-158). The outlet of the pump was back-pressure regulated to maintain a 25 sccm sampling flow pre-concentrating 500 mL of sample at ~1 atm on a multi-bed sorbent trap held at around -130℃ in a custom built unit (described in Warburton et al., 2025), flow controlled by a downstream mass flow controller (Alicat MC). All samples were de-humidified with a -40℃ water trap. After removal of CO_2 and other permanent gases at -80℃, the preconcentration trap was desorbed and refocussed at -130℃ before desorption onto a WAX GC column (Agilent VF-WAX-MS 60 m, 0.25 mm I.D. 150 µm film). Analytes not retained on the WAX column (C2 - C6 aliphatics) were diverted by Deans Switch and separated on a PLOT column (Agilent Al2O3/Na2SO4 50 m, 0.32 mm I.D. 5 µm film) then quantified using a flame ionisation detector (FID, Agilent 7890B). Oxygenates, >C6 aliphatics and aromatics were not diverted and eluted from the WAX column where the flow was split around 3:1 between an FID and a quadrupole mass spectrometer (Agilent 5977). A 30-component ozone precursor mix from NPL (nominally 4 ppb) was used to quantify the non-methane hydrocarbons reported by FID and was sampled at the beginning, middle and end of the reporting period. Oxygenated VOCs, and any compounds reported from the Mass Spectrometric detector, were calibrated more frequently (every 15 samples) using a different NPL certified mix in the 1 ppm range. OVOC calibrations were diluted using a combination of mass flow controllers mixing the blank gas with the high concentration standard to generate near-ambient concentrations of each component. Benzene, a component in both calibration mixtures, was used to unify the calibration scale and overcome the uncertainties caused by the dilution set-up. VOC free blanks were created from compressed air, catalytically scrubbed using 1% Pt on Alumina beads at 375°C.

Continuous, mixing ratios of light volatile organic compounds (C_2–C_6 non-methane hydrocarbons), carbonyl sulfide, and over 50 halocarbons were determined in-situ using an automated Medusa gas chromatograph–mass spectrometer (Medusa GC-MS, hereafter referred to as Medusa) system integrated into the global AGAGE (Advanced Global Atmospheric Gases Experiment) network (Prinn et al., 2018). To achieve sub-ppt detection limits, a 2.0 L ambient sample was filtered, dried, and routed through a custom dual-trap preconcentration module at -165°C using a helium compressor system before thermal desorption. Chromatographic separation of the sample was achieved on a GC (Agilent 6890) fitted with a CP-PoraBOND Q, 0.32 mm ID_25 m, 5 µm, (Agilent) capillary column, followed by detection via a quadrupole mass spectrometer operated in selective ion monitoring (SIM) mode (Agilent MSD 5975B). To ensure good long-term stability and full compliance with network data quality objectives, instrumental drift and sensitivity shifts were dynamically corrected by bracketing every ambient measurement with a compressed working gas standard.

For the analysis, only compounds that were above the limit of quantification (LOQ) were considered, and compounds in common for both Medusa and GC-FID/MS were averaged. Table S1 provides the list of the compounds quantified by these

https://doi.org/10.5194/egusphere-2026-6814
Preprint. Discussion started: 12 November 2026
© Author(s) 2026. CC BY 4.0 License.

instruments and their families, hereafter reported as carbonaceous trace gases (CTG). In this work, carbonaceous trace gases exclude CO_2, CO and CH_4.

2.4.3 Vocus-PTR-MS

Additionally, VOCs were measured using a Vocus proton-transfer-reaction mass spectrometer (PTR-MS, hereafter referred to as Vocus) with H_3O^+ as the reagent ion (Krechmer et al., 2018). The instrument was configured with a reduced electric field strength (E/N) of 131 Td and the temperature of the focusing ion molecular reactor (FIMR) set to 60°C at a pressure of 2 mbar. To assess the instrument background, automatic measurements of zero air were performed in regular intervals. Data from the Vocus is only available starting 26.8 and until 17.9.

Vocus clustering and family assignment

Families were assigned as the following groups: CH, CHO, CHN, CHON, CHOS, CHONS, halogen-containing, siloxanes and others. While the Vocus was regularly calibrated using a standard bottle of quantified VOCs, issues in the automated calibration sequence of the Vocus software (v1.16.5) resulted in irreproducible changes to instrument conditions exclusively during calibration periods. Therefore, an absolute concentration calibration of the data was not possible. However, since the mass calibration was unaffected, relative signal variability and molecular formula assignment is robust. The VOC signals were therefore treated as centered z-scores and a partitioning clustering was applied using shape-based-distance.

Log10 *C calculation at 300K from molecular formula of VOC (Vocus)**

$$log_{10}C^* = (n_C^0 - n_C)b_C - n_O b_O - 2\frac{n_C n_O}{n_C + n_O}b_{CO} - n_N b_N - n_S b_S \quad (6)$$

With n^0_C the reference carbon number n_C, n_O, n_N and n_S being the number of C, O, N and S for each molecular formula. b_C, b_O, b_N and b_S correspond to the contribution of each atom to $\log_{10}C_0$ (Li et al., 2016), and b_{CO} is the carbon-oxygen nonideality (Donahue et al., 2011).

To calculate *C** values at 273.15K, the following equation was used (Clausius Clapeyron equation):

$$C_i^0 = C_i^0(T_{ref})\exp[\frac{\Delta H_{vap,i}}{R}(\frac{1}{T_{ref}} - \frac{1}{T})] \quad (7)$$

Volume mixing ratios obtained for the gaseous species in ppbC were converted into mass concentration in µgC m^{-3} according to Eq (8):

$$\mu gC\ m^{-3} = ppbC\frac{0.012 * P}{T * R} \quad (8)$$

With P = 65300 Pa, R = 8.314 J mol^{-1} K^{-1}, T = 273.15 K

https://doi.org/10.5194/egusphere-2026-6814
Preprint. Discussion started: 12 November 2026
© Author(s) 2026. CC BY 4.0 License.

2.5. Auxiliary measurements

Atmospheric radon-222 (^{222}Rn) activity concentrations at the Jungfraujoch station were monitored continuously as part of the Integrated Carbon Observation System (ICOS) with a two-filter dual flow loop instrument (Whittlestone and Zahorowski, 1998). The instrument determines radon activity at an hourly time resolution by quantifying the alpha decay of radon-222 daughters formed within a 750 L detector volume (Griffiths et al., 2014), with data made available through the ICOS data portal https://data.icos-cp.eu/portal/.

Standard meteorological parameters were continuously recorded by MeteoSwiss using high-altitude ruggedized instrumentation. Essential variables, including temperature, relative humidity, atmospheric pressure, and wind dynamics were measured automatically via the national SwissMetNet network at 10-minute and hourly time resolutions and are available openly through the MeteoSwiss Open Data Portal.

2.6. Air mass identification

2.6.1 Separation of FT vs PBL

Following Brunner et al. (2021), the probability of free-tropospheric origin, P_{FT}, was calculated from N90 and ^{222}Rn activity concentrations (Text S1). Periods with $P_{FT} \geq 0.7$ were classified as FT, and periods with $P_{FT} < 0.3$ as PBL-influenced (PBLi). Periods with $0.3 \leq P_{FT} < 0.7$ as well as periods lacking the required input data were not assigned an air mass condition. Wildfire and dust events were identified separately using the criteria in Section 2.6.2; and the event demonitation prevailed over the FT/PBLi. Instrument coverage differed between air-mass categories (Fig. S2). In particular, Vocus measurements covered neither wildfire event, and quantified CTG data were unavailable for the North American wildfire plume. Comparisons therefore describe the available measurement periods rather than a fully matched campaign-wide dataset.

2.6.2 Identification of wildfire and dust plumes

Wildfire events were identified by benzene and CO concentrations. Gaseous concentration enhancements compared to background conditions (5th percentile of monthly data) were calculated and the plumes were identified by inspection of elevated CO and benzene levels. In addition, source footprints and fire inventories (https://effis.jrc.ec.europa.eu/apps/firenews.viewer/, https://firms.modaps.eosdis.nasa.gov/usfs/map/#t:tsd;d:2022-09-08..2022-09-15;l:fires_all,fire-perimeter,countries,earth;@-104.6,40.0,4.1z) were further used to confirm the geographic origin of the fires. The first identified wildfire plume reached Jungfraujoch between 17 and 18 August and came from Europe, while the second one was on 18-19.09.2022 and came from North America (Fig. S7). Their physical age was estimated, based on Flexpart age calculated for fire BC, to be around 1.6 days for the plume from Europe and 10 days for the one from North America (https://flexpart-request.nilu.no/data-access, last access: 06.05.2026; Giglio et al., 2013).

One dust event was identified on September 13-14 based on the concentration of coarse mode particles (PM_{10}-PM_1), a negative Angstrom exponent of the single scattering albedo and dust forecast (Collaud Coen et al. (2026, 2004);

https://doi.org/10.5194/egusphere-2026-6814
Preprint. Discussion started: 12 November 2026
© Author(s) 2026. CC BY 4.0 License.

http://www.bsc.es/projects/earthscience/visor/sub_fc8.php?dom=med8&type=sfc&vyear=2022&vmonth=09&vday=14&vhour=12#;Fig. S8). The conditions and air masses over the campaign are summarized in Table 3.

Table 3: Air mass types detected during the campaign period.

Air mass	Abbreviation	Identification criterion	Dates	Total time [h]
Free troposphere	FT	^{222}Rn & N_{90}		199
Planetary boundary layer intrusions	PBLi	^{222}Rn & N_{90}		427
Wildfire plume from Europe	wildfire EUR	benzene, CO, source footprints, fire inventories	17-18.08.2022	28
Wildfire plume from North America	wildfire NA	benzene, CO, source footprints, fire inventories	18-19.09.2022	26
Saharan dust plume	dust	Angstrom exponent of single scattering albedo and PM_{10}-PM_1	13-14.09.2022	29

2.7. Site-specific considerations

Touristic activities and the related maintenance and construction activities result in local pollution on Jungfraujoch. This pollution typically shows a clear diurnal and meteorologically dependent pattern and can be partially tracked by additional measurements at the adjacent Jungfraujoch East Ridge site (Affolter et al., 2021; Bukowiecki et al., 2021), which is not accessible to tourists. The East Ridge site is equipped with a CPC and an AE33, the particle number concentration timeseries was carefully compared for both sites. In the present work, only major events that produced a significant impact on the hourly averaged data were flagged by post manual user inspection. This approach is conservative, at least for particulate pollution, as local contamination from touristic activities usually has a greater impact on particle number than on quantities related to particulate mass concentration. An exception was made for VOCUS and GC VOC data, for which unflagged data were retained in order to explore possible impact of local pollution on VOC concentrations. All data were treated at the local laboratory conditions (with a pressure of about 655 h Pa, except for FATCAT (650 Pa) and for the conversion of ppb to µg m^{-3} for the GCs (see Section 2.4.) and a temperature of 298.15 K) and were not corrected to standard temperature and pressure (STP).

https://doi.org/10.5194/egusphere-2026-6814
Preprint. Discussion started: 12 November 2026
© Author(s) 2026. CC BY 4.0 License.

3 Results and discussion

3.1 Overview of the main carbonaceous species during the campaign

The average carbon-equivalent concentrations of the carbonaceous species measured during the campaign span over several orders of magnitude. CO_2, CH_4, and CO showed the highest concentrations, with $1.4 \cdot 10^5$, $6.8 \cdot 10^2$ and 33 µg C m^{-3} on average, respectively. Quantified carbonaceous trace gases (CTG), which included NMHCs, OVOCs, carbonyl sulfide (COS) and inorganic halogenated compounds, showed on average a concentration of 2.3 µg C m^{-3}. However, it should be noted that a fraction of VOCs cannot be detected by gas chromatography or PTR-MS, such as IVOCs. Additionally, a fraction that could be detected by the instruments deployed could not be quantified. Therefore, the above value for CTG presents a lower limit and the uncertainty on this value is high. Particulate organic carbon accounted for 0.3 µg C m^{-3}, while particulate BC, quantified here as eBC (Section 2.2.3), showed the lowest concentration of 0.05 µg C m^{-3} on average.

The remainder of this section provides an in-depth overview of CTGs, pOC and BC measured during the campaign.

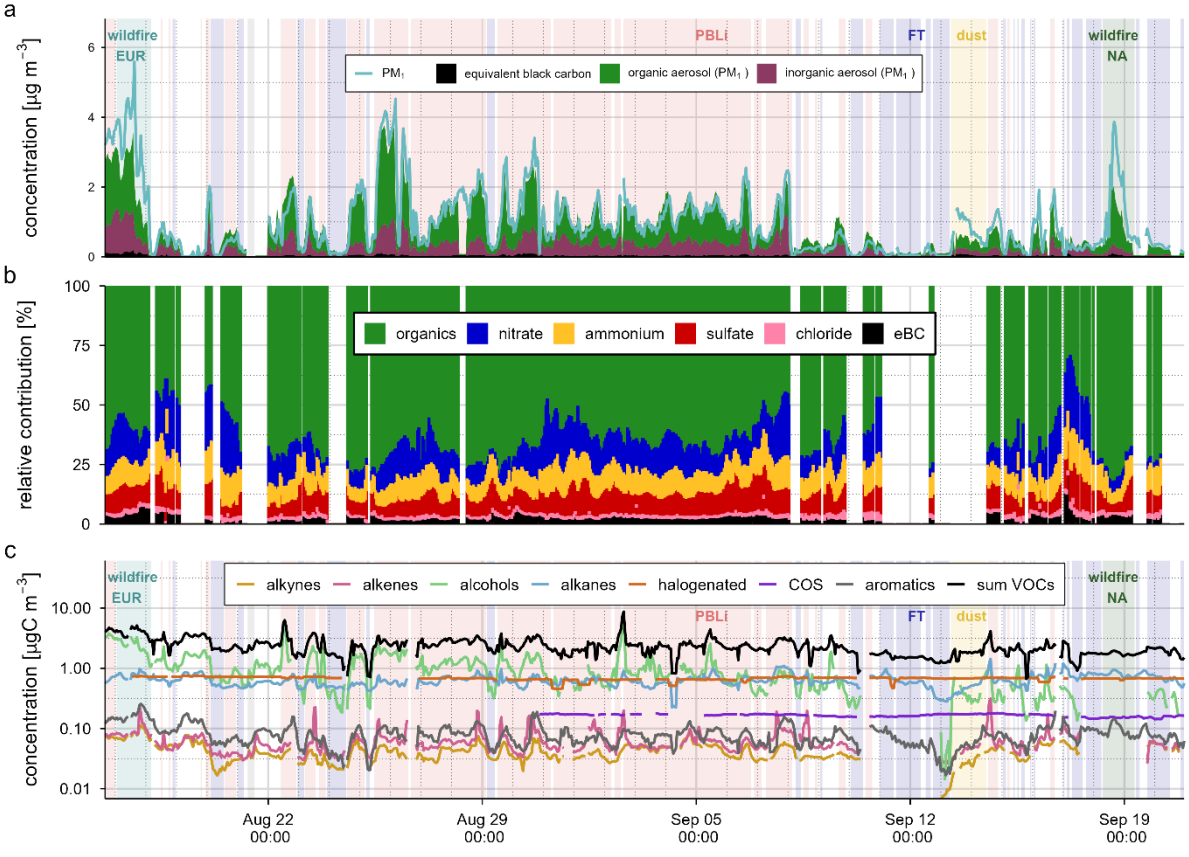


Figure 1: Timeseries of PM_1, its constituents, and carbonaceous trace gases during the campaign (1 h averages). (a) PM_1 mass concentration and composition (PM_1 is measured by Fidas and scaled to match campaign average fine mode mass derived from MPSS), particulate equivalent black carbon mass from MAAP, particulate organic and inorganic mass from PM_1-ToF-ACSM (scaled to the average fine mode mass derived from the MPSS by a CE factor of 1). (b) Relative chemical composition of PM_1 obtained

https://doi.org/10.5194/egusphere-2026-6814
Preprint. Discussion started: 12 November 2026
© Author(s) 2026. CC BY 4.0 License.

from PM_1-ToF-ACSM and MAAP measurements. (c) Carbonaceous trace gases (CTGs) measured by Medusa-GC and GC-FID/MS, note the log scale. Periods with identified air mass type are shown as background colours in (a) and (c). To avoid negative values in stacked plots, values below LOD in panels (a) and (b) were replaced with the LOD.

Figure 1 a. shows the timeseries of total PM_1 along with its main constituent components: organic aerosol, inorganic salts and black carbon. The total PM_1 concentrations were measured by the Fidas and scaled, using an averaged factor of 2.4, to PM_1 derived from the MPSS measurements (assuming spherical particles with a composition-dependent density calculated using Eq. 1), because the Fidas proprietary algorithm was found to overestimate PM_1 concentrations by this factor (Fig. S3b), and the MPSS measurements agreed well in terms of both number and mass with independent measurements obtained by the CPC, MAAP and ACSM (Figs. S3a and c). Total PM_1 concentrations were mostly below 5 µg m^{-3}. This is consistent with Fröhlich et al. (2015), who measured PM_1 concentration at JFJ in the summer below 1 µg m^{-3} in the night and morning and about 2-6 µg m^{-3} in the afternoon and evening, with peaks up to 9.6 µg m^{-3}.

Figure 1 b. shows the relative chemical composition of PM_1 from ACSM and MAAP measurements over time. PM_1 was dominated by OA most of the time, whereas inorganic fraction exceeded 50% only during few short episodes, e.g. on September 17th, when the total PM_1 concentration was low (0.18-0.37 µg m^{-3}). Such high organic fraction in PM_1 during the summer season is consistent with previous observations at Jungfraujoch (Bukowiecki et al., 2016; Weng et al., 2026).

Figure 1 c. presents the timeseries of the major CTG families measured by GC. Three GCs (AirmoVOC, GC-FID/MS and Medusa GC-MS) were used to quantify trace gases, including NMHCs and OVOCs up to C20. In addition, a Vocus was deployed to obtain high sensitivity VOC information for a broad compound range at high-time-resolution. The AirmoVOC GC (Chromatotec, France) should have been able to detect C6 to C20 VOCs, including linear alkanes and gaseous polycyclic aromatic hydrocarbons (PAHs) from naphthalene to benzo(a)pyrene, according to the manufacturer and to the calibration performed. Unfortunately, even after calibration and sampling a homemade PAH mixture, it was not possible to identify these compounds in the ambient air samples; only benzene could be quantified. The GC-FID/MS and the Medusa GC-MS measured 97 compounds, of which 66 were above the instruments' limits of quantification (LOQ). These compounds are reported in Table S1 and grouped by their families. Eight of them were in common between both instruments. The concentrations of some of these co-measured species (benzene, ethane, i-pentane, n-pentane) agreed well for the two instruments, while the concentrations of others (i-butane and n-butane) differed substantially (Fig. S9).

The Vocus detected 403 ions; however, only their relative temporal variability could be determined whereas concentrations could not be quantified. Therefore, we report their temporal variability as z-scores, i.e. variability of ion signal intensities, expressed as number of standard deviations, around their mean values (Fig. S10). The temporal variability of toluene z-scores from the Vocus agreed well with those measured by the Medusa GC-MS, which gives some confidence when interpreting relative changes in the Vocus data. On the other hand, there was a poorer agreement for benzene between both instruments.

https://doi.org/10.5194/egusphere-2026-6814
Preprint. Discussion started: 12 November 2026
© Author(s) 2026. CC BY 4.0 License.

Given that about a third of the CTG species were below the instrument LOQs and the inability to quantify the Vocus measurements, the sums of the quantified CTG concentrations displayed in Fig. 1 only represent a subset of total CTGs at Jungfraujoch, and it remains elusive by how much total CTG concentrations exceed the quantified portion. Overall, the CTG concentrations were mostly between 1.5 and 5 µg C m^{-3}, with rare but intense spikes up to 8.7 µg C m^{-3} caused by increases in the concentrations of alcohol species. The composition of quantified CTGs was dominated by alcohols and alkanes, in particular methanol and ethane (0.75 and 0.45 µg C m^{-3} on average, respectively; Table S1). In contrast, aromatics, alkenes and alkynes had very low measured concentrations, which can be expected given the site's remoteness and their relatively short lifetimes (few hours to few weeks for acetylene). Other high-altitude sites also reported NMHC or VOC concentrations to be dominated by alkanes at Monte Cimone (Vullo et al., 2016) and on the Tibetan Plateau (Wu et al., 2025) while in Izana, NMHCs were dominated by ethane (Fischer et al., 1998). Halogenated compounds and COS showed very stable concentrations with little influence from the different air masses, which is due to their very long lifetime (COS: 2-3 yrs, halogenated up to 300 yrs; Aydin et al., 2008; Jobson et al., 1999; Montzka et al., 2007). Due to the presence of these long-lived compounds, the measured CTG concentrations were very rarely below 1 µg C m^{-3} (min 0.67 µg C m^{-3}). This is in contrast to particulate matter, which has short lifetime in the troposphere (min PM_1 during FT periods and at night as low as 0.0046 µg C m^{-3}).

https://doi.org/10.5194/egusphere-2026-6814
Preprint. Discussion started: 12 November 2026
© Author(s) 2026. CC BY 4.0 License.

3.2. Atmospheric composition for different air masses

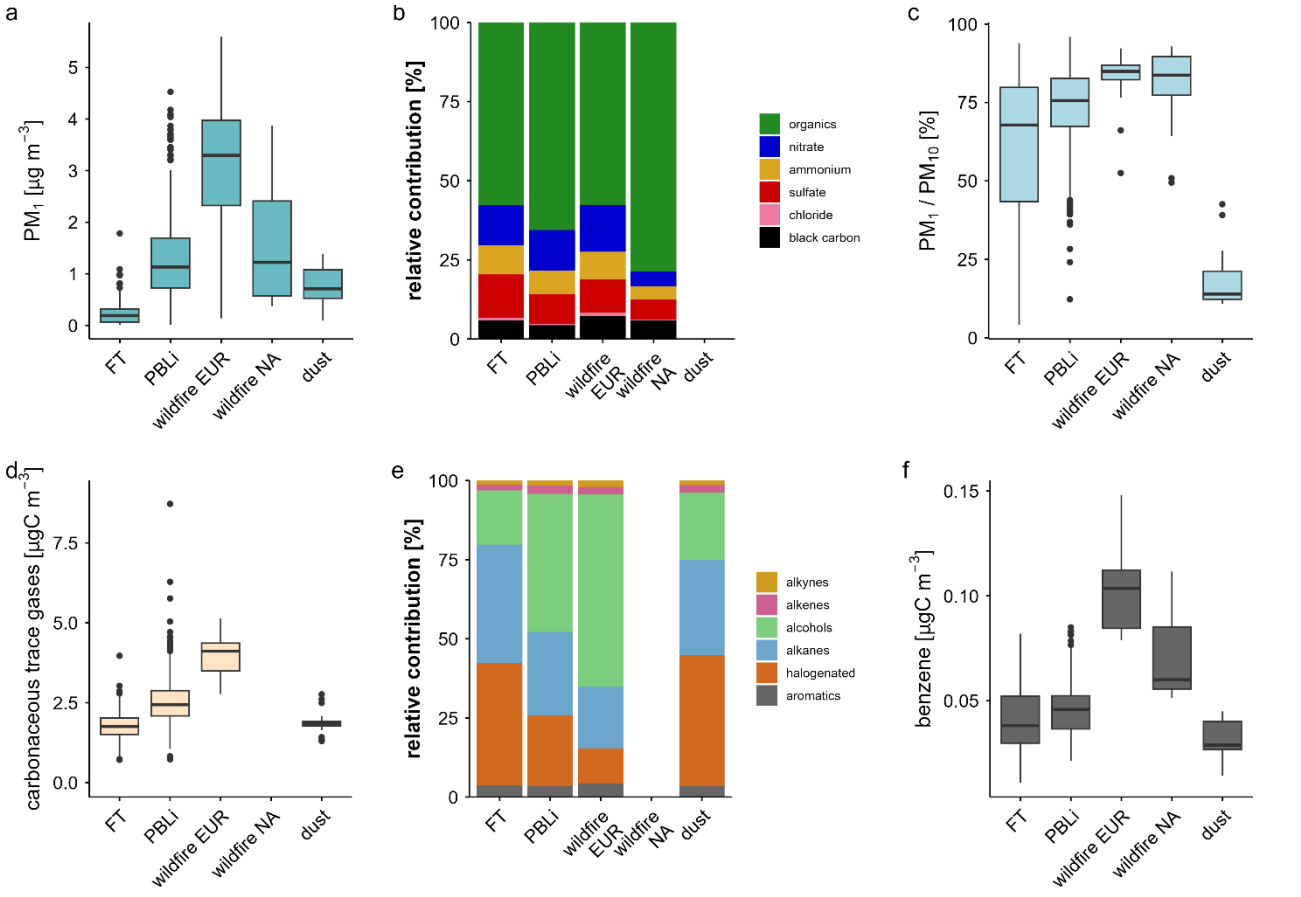


Figure 2: Observed particulate matter and carbonaceous trace gases for the different air masses encountered during the campaign. (a) Boxplots (centre line: median; box limits: 25th and 75th percentile; whisker length: extend from the hinge to the largest or smallest value respectively, up to 1.5 times interquartile range) of PM_1 concentrations, (b) mass fractions of PM_1 species, (c) boxplots of PM_1-to-PM_{10} ratios from raw Fidas output, (d) boxplots of total quantified carbonaceous trace gases, (e) relative contributions of VOC families, and (f) boxplot of benzene. Note the missing data for the wildfire NA case in panels (d) and (e).

Different types of air masses were encountered during the campaign as described in Section 2.6 and summarized in Table 3. In this section we characterize the concentrations and properties of particulate and gaseous carbon in these different air masses. The site was influenced by PBLi about 50% of the time and FT conditions about 23% of the time. In addition, dust and wildfire plumes were encountered. Atmospheric composition differences between the air masses and plume events will be discussed in the following based on Figure 2, which presents PM_1 and CTG concentrations and relative composition segregated by air mass types.

https://doi.org/10.5194/egusphere-2026-6814
Preprint. Discussion started: 12 November 2026
© Author(s) 2026. CC BY 4.0 License.

3.2.1. FT vs PBLi

Free tropospheric conditions were characterised by the lowest concentrations for both PM_1 and CTG (Figures 2a. and d), as expected, although the lowest VOC concentrations remained proportionally higher than the lowest PM_1 concentrations due to the presence of long-lived COS and halogenated species (Section 3.1). PM_1 was dominated by organics for all air masses encountered during the summer season (Fig. 2b), but the relative contribution of SO_4^{2-} slightly increased for FT (14%) compared to PBLi (9%), as previous reported for JFJ (Bukowiecki et al., 2016; Fröhlich et al., 2015). During FT conditions, VOCs were dominated by halogenated species (34%) and alkanes (30%), while alcohols made up 22% (Fig. 2e). On the other hand, PBLi conditions were characterized by lower contributions of inorganic aerosols, halogenated species and alkanes, and higher contributions of organic aerosol, methanol and ethanol (40%). The higher relative contributions in the FT of alkanes and halogenated compounds can be explained by their much longer lifetime in the atmosphere (ethane: 41 days, halogenated 3.6 d-300 yrs; Jobson et al., 1999) than more reactive species such as alcohols and aromatics (toluene: 2 days to methanol 12 days; Atkinson, 2000). The low contribution of alcohols in the FT could also be due to unquantified GC-FID/MS data, in particular between September 10 and 12.

3.2.2. Wildfires

The highest PM_1 concentrations recorded during the campaign occurred during the European wildfire event. The wildfire from North America brought PM_1 concentrations that were similar to or higher than median PBLi concentrations. Median CTG concentration were also highest for the European wildfire event, although CTG data are not available for the North Amercian wildfire plume. This provides an example of the impact that long-range transported wildfire smoke can have on particulate and gaseous pollution levels far from source.

The relative contribution of OA was substantially lower (58%) for the European wildfire event than the North American wildfire event (79%). On the other hand, BC and inorganic NR-PM_1 contributions were higher for the wildfire from Europe (7.3% and 35%, respectively) compared to the wildfire from NA (5.9% and 15%, respectively). The higher relative OA contribution during the North American event could be explained by less mixing of the plume with PBLi, as these plumes are usually transported in the free troposphere (Ortiz-Amezcua et al., 2017), as well the formation of aged and secondary OA during the longer transport time of the NA than EUR plume, resulting in less absolute OA mass loss compared to inorganic aerosol (Garofalo et al., 2019).

The gas phase species benzene, which originates from general combustion processes, can serve as a useful indicator for the detection of wildfire smoke at remote sites like the JFJ. Benzene increased substantially during both wildfire events in this campaign, with higher values measured in the European than the North American plume (Fig. 2f). This difference can be at

https://doi.org/10.5194/egusphere-2026-6814
Preprint. Discussion started: 12 November 2026
© Author(s) 2026. CC BY 4.0 License.

least partially explained by the reactive loss of benzene during transport, with the NA plume originating from further away and having a higher plume age.

The longer transport time and higher age of the NA plume relative to the EUR plume was evidenced by the ratios of toluene/benzene, and aerosol species (organics, inorganics, and BC) to CO displayed in Fig. S11. The toluene/benzene ratio was higher for the EUR than the NA plume since toluene has a shorter lifetime than benzene (Atkinson, 2000). Similarly, the ratios of aerosol species to CO were all higher for the EUR than the NA plume, which reflects the longer lifetime of CO relative to the aerosol species (Yokelson et al., 2009). This difference between the EUR and NA plumes was greater for the inorganics-to-CO ratio than the organics-to-CO ratio, which is consistent with the relative fractions displayed in Fig. 2b and discussed above.

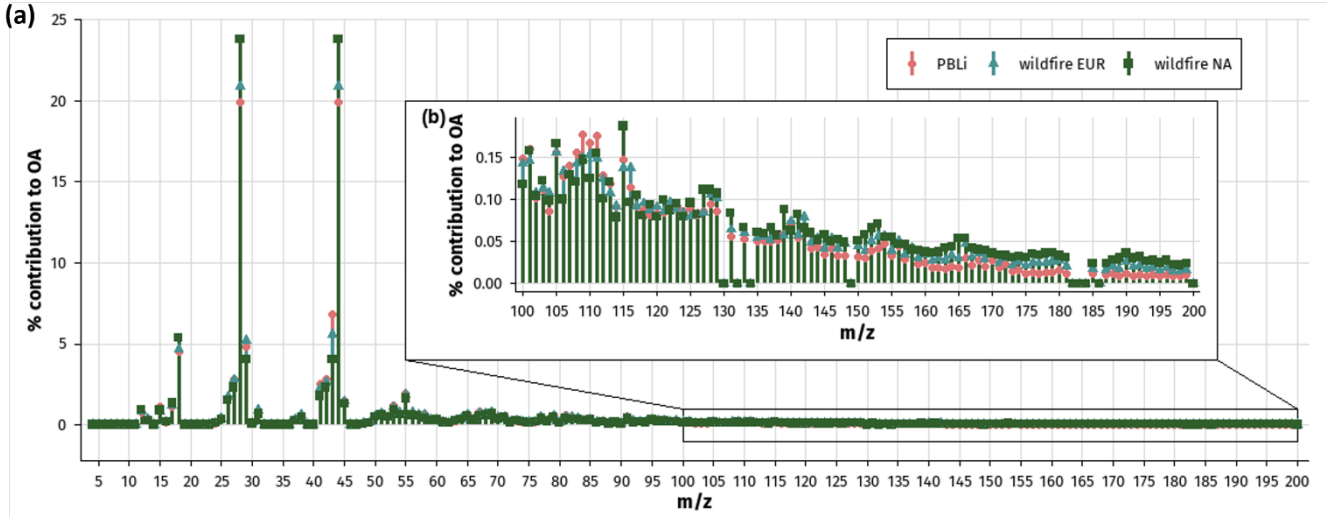


Figure 3: Chemical fingerprints of the organic aerosol (OA) from the two wildfire plumes and PBLi conditions. (a) Whole mass spectrum (ToF-ACSM) of OA with (b) zoom into fragment ions with *m/z* above 100.

To further investigate the chemical composition of these plumes compared to PBLi, the mass spectra obtained for OA from the ACSM were averaged for PBLi conditions and both wildfire events (Figure 3). The observed degrees of oxidation, as illustrated by the intensities of *f*43 (*m/z* 43 concentration divided by OA concentration) and *f*44, differed between PBLi and the two wildfire events, with most aged OA from wildfire from North America (higher *f*44) and least aged from PBLi, as expected based on their geographical origins. Figure 3b. presents a zoom into $m/z > 100$, which shows overall higher levels of these *m/z* (e.g., 115, $m/z \geq 135$) for the wildfire plumes, especially the one from North America. A similar observation was made for biomass burning (BB) plumes in the US, where the fraction of ions larger than 100 amu contributed 11% to the organic signal during BB plumes, compared to 5% during periods of non-BB influence (Zhou et al., 2017). Figure S12, which shows the contribution of *m/z* 100 to 200 to the sum of these *m/z*, further highlights the difference between *m/z* 100-135, mainly

https://doi.org/10.5194/egusphere-2026-6814
Preprint. Discussion started: 12 November 2026
© Author(s) 2026. CC BY 4.0 License.

dominated by PBLi, and *m/z* 135-200, dominated by the wildfires. These enhanced high-*m/z* organic fragments coincided with lower inferred OA volatility in the wildfire plumes, particularly the North American plume.

3.2.3. Dust

PM_1 constituted most of PM_{10} throughout the measurement campaign, except for a short spike on September 1st and during the dust event, where it fell below 25%, as PM_{10} increased up to 12.5 µg m^{-3} (Fig. 2c, Fig. S13). The number and volume size distributions averaged per air mass type (Fig. S14) showed the presence of larger particles during the dust event. PM_1 and CTG concentrations were low during this event. The CTG composition was very similar to free tropospheric conditions, with a lower contribution of alcohols than for PBLi and wildfire EUR, which could indicate that the station was under free tropospheric conditions and that the dust plume travelled in the FT. The relative chemical composition of the dust aerosol could not be reliably measured with the available instruments for two main reasons: i) Dust is refractory, hence the ACSM cannot measure the tail of the dust mass distribution extending down to fine mode diameters. ii) Dust is weakly light absorbing, thus incurring a positive measurement artefact in eBC mass concentration when dust mass exceeds BC mass by orders in magnitude during dust events, so it was omitted on Figure 1b and Figure 2b (Collaud Coen et al., 2026).

3.2.4. Local emissions

The ambient concentrations were affected by local pollution due to the research station being part of the Jungfraujoch facilities which primarily serve touristic activities (Section 2.7.). The aerosol contamination signal, which quite well-known (Bukowiecki et al., 2016; Fröhlich et al., 2015), has been removed from the aerosol data as described Section 2.7. By contrast, the Vocus data was used to identify locally emitted VOCs and to investigate their potential impact on the VOC emissions measured at Jungfraujoch. The Vocus was partially operating during the campaign, so the wildfire plumes were unfortunately not covered. A clustering approach was chosen to separate locally emitted VOCs from those transported to the site. Specifically, the time series of Vocus signals, expressed z-scores (see Section 2.4.3), were grouped into 4 different clusters (Figs. S15 and S16) using partitioning clustering with a shape-based distance, in order to identify similar patterns in their timeseries.

https://doi.org/10.5194/egusphere-2026-6814
Preprint. Discussion started: 12 November 2026
© Author(s) 2026. CC BY 4.0 License.

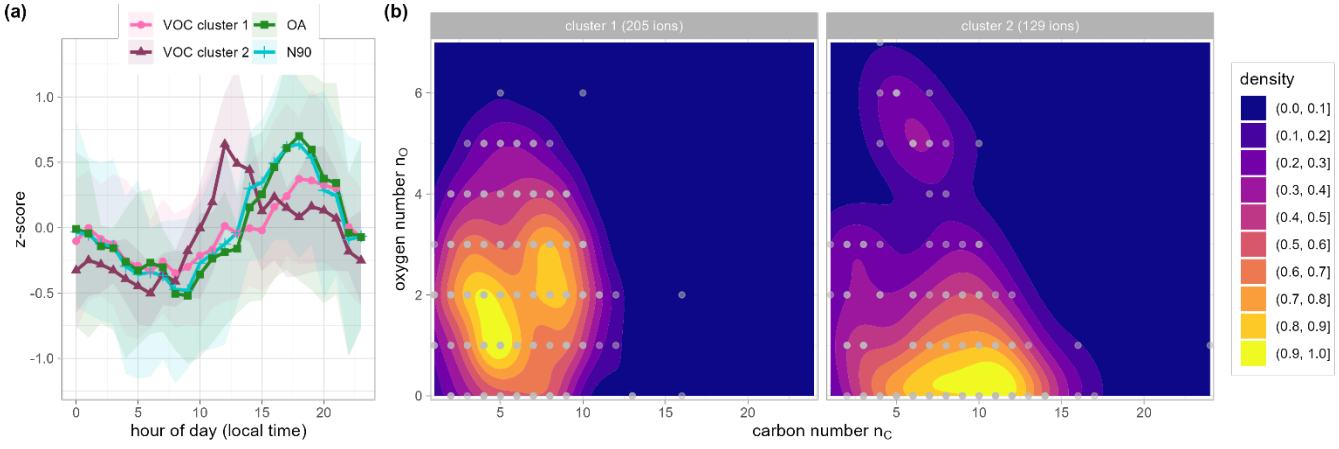


Figure 4: Results of the cluster analysis performed on the VOC time series measured by the Vocus PTR-MS. (a) Diurnal plots of VOCs clusters 1 and 2 along with organic aerosol (OA) from the ACSM and N90 from the SMPS. Lines represent the median value and shaded areas represent 25-75th percentile. (b) Two-dimensional density plot of the carbon and oxygen number of the ions assigned to clusters 1 and 2.

Clusters 1 and 2 contained most of the ions and show distinct variabilities (Fig. S15 and S16). Cluster 3 was very likely an instrumental artifact which decreased quickly at the start of the campaign (Fig. S16) and contained mainly N-containing species (Fig. S15). Cluster 4 could originate from a marine source as it peaked together with $CHBr_3$ and CH_2Br_2 (measured by the Medusa-GC-MS), which have almost no continental source, but its temporal variability is unclear, and we will therefore focus on clusters 1 & 2. The diel cycle of cluster 1 peaked in the late afternoon (Fig. 4a.) and correlated strongly with N90 (ρ=0.84; Fig. S17), which indicated that it could be transported to the site by the PBLi. Cluster 2 peaked around noon (local time) and increased concurrently with the particle number concentration (Fig. S18), which is affected by local contamination. The diel cycles of clusters 1 and 2 were similar to the ones obtained by Fröhlich et al. (2015) for OA constituents associated with PBLi and local emissions from touristic activities, respectively. Moreover, cluster 1 contained compounds with lower carbon number and higher oxygen number than cluster 2 (Fig. 4b.), in line with being chemically altered during atmospheric transport, while cluster 2 contained long-chain, low oxidized compounds more representative of fresh emissions. In particular cluster 2 contained some short- (acetaldehyde, acrolein) and long-chain aldehydes (heptanal, octanal, nonanal, decenal and undecanal), that were linked to cooking activities (Coggon et al., 2024; Klein et al., 2016), as well as ethanol, D5-siloxanes and D4-siloxanes, which are associated with volatile chemical product (VCP) emissions (Coggon et al., 2024). Ethanol measured by the GC was also observed to increase in intense spikes during the day, often when the CPC also spiked (Fig. S18). Cluster 2 was thus likely not representative for a site in the lower free troposphere with PBL intrusions but rather indicated the influence of local touristic activities (restaurants, cigarette smoke, personal care products) at the site. This shows that these activities impact both aerosol and gas phase and makes flagging necessary for data sets intended to represent the chemical composition of the atmosphere at a remote mountain station. Note however that without quantification and with high uncertainties on these results, conclusions are limited.

https://doi.org/10.5194/egusphere-2026-6814
Preprint. Discussion started: 12 November 2026
© Author(s) 2026. CC BY 4.0 License.

3.3. Mass closure of total particulate carbon (TC)

Four independent techniques were used to quantify total particulate carbon (TC) and its organic (OC) and elemental (EC) fractions: (i) thermo-optical analysis of 24 h hi-Vol filters (TOA, referred to here as TC_{TOA}), (ii) the TCA instrument (TC_{TCA}, hourly), (iii) the FATCAT analyser (TC_{FATCAT}, 2h, resampled to 1h), and (iv) the $TC_{ACSM+MAAP}$ representing the sum of OC measured online by the ACSM (converted to OC with an average OA : OC ratio of 2.40 ± 0.6) and eBC measured by the MAAP. The time series of daily-average TC values from each of the four techniques are displayed in Figure 5a, and a scatter plot of TC from each technique against the mean TC of the four techniques is shown in Figure 5b.

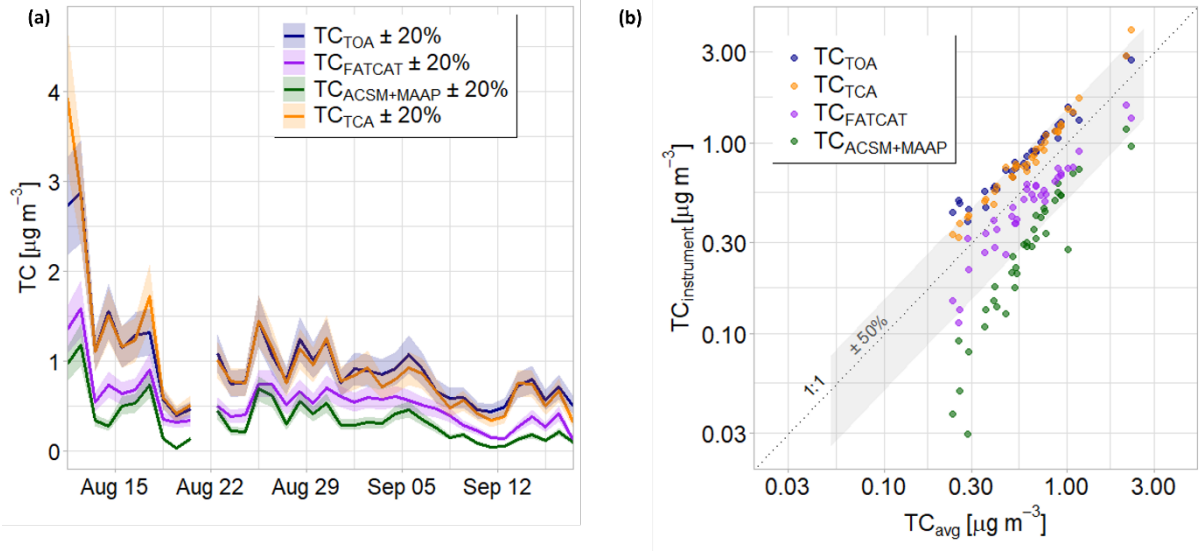


Figure 5: Mass closure of total particulate carbon (TC) for the four different methods (TOA, TCA, FATCAT and ACSM+MAAP). (a) Temporal variability of TC throughout the campaign for the four methods. (b) TC from each technique versus TC averaged from the four techniques. The data from online instruments (TCA, FATCAT, ACSM, MAAP) was averaged to match the daily resolution of the TOA.

Total particulate carbon (TC) concentrations at Jungfraujoch were generally < 2 µg m^{-3}, with only a few elevated values at the beginning of the campaign. At such low levels, all measurement techniques operate close to their detection limits and are therefore susceptible to method-specific artefacts e.g. imperfect background subtraction, filter-blank uncertainties, and limited signal-to-noise ratios. Consequently, no single approach can be taken as a definitive reference.

The four TC estimates exhibited similar temporal patterns (Fig. 5a), but agreement in absolute concentrations varied between method pairs. TC from TOA and TCA agreed within a factor of 1.06 (R^2 = 0.97), whereas TC from FATCAT and ACSM + MAAP agreed within a factor of 1.40 (R^2 = 0.92) although with closer agreement at higher concentration levels. TOA and TCA generally yielded approximately twice the concentrations obtained by the other two approaches, with larger relative discrepancies below 0.5 µg C m^{-3}. Figure 5b shows that each method agrees within ±50% with the mean of all methods for the concentration range > 0.5 µg C m^{-3}. Because the mean in Fig. 5b includes the method plotted against it, these comparisons are not independent; pairwise comparisons for 1h-averages measured by the three online-methods are provided in Fig. S19c-e.

https://doi.org/10.5194/egusphere-2026-6814
Preprint. Discussion started: 12 November 2026
© Author(s) 2026. CC BY 4.0 License.

These show that precise measurements at 1h time resolution are possible for atmospheric TC concentrations larger than ~0.5 µg m^{-3}, whereas random noise and systematic errors increase for lower concentrations.

To identify the origin of these differences, OC and EC were examined separately (Fig. S19a and b). Offline OC from the thermo-optical analysis (OC_{TOA}) correlated well with ACSM-derived OC but was consistently higher due to an offset between the two methods (Fig. S19a). EC was estimated from three sources: eBC measured by the filter-based MAAP (and the AE33, although only MAAP is shown because it is less affected by filter-loading artefacts), refractory BC from the SP2 (rBC), and EC_{TOA} from the TOA protocol. EC_{TOA} agreed reasonably with the daily-averaged eBC-MAAP, whereas rBC was systematically lower (Fig. S19b). Because EC represented only ~5 % of TC on average, the observed TC discrepancies were mainly driven by the methods used to determine TC and OC.

Potential contributors to the mismatches, especially at low concentrations, include but are not limited to: (i) zeroing / background subtraction and gas-phase artefacts in the total-carbon analysers but also for the filter-based TOA, (ii) ACSM-related uncertainties such as collection efficiency and the OA : OC conversion factor, together with aerodynamically limited PM transmission window; and (iii) noise/ stability and linearity issues at low concentrations. The strong correlations indicate that the methods captured similar temporal variability, but the systematic differences in absolute concentrations prevent a conclusion of quantitative closure across all four approaches. These results support relative comparisons, while absolute closure requires further evaluation of method-specific biases and measurement uncertainties in this low-concentration environment.

3.4. Volatility

3.4.1. Total particulate carbon volatility

In addition to providing total carbon concentrations, the FATCAT also provides thermograms of the carbon release rate as a function of elapsed heating time (a proxy for filter temperature; Figure 6). Compounds with higher volatility volatilize earlier than ones with lower volatility. The FATCAT volatility classes defined here — high (<20 s), intermediate (20–35 s), and low/refractory (>35 s) — are operationally defined boundaries chosen to illustrate the capability of FATCAT thermograms to discriminate between aerosol sources, rather than representing absolute physicochemical thresholds, which is consistent with the thermogram interpretation framework discussed in Keller et al. (2023) and Corbin et al. (2024). As a complementary example, Fig. 6 also includes a local fossil fuel contamination event recorded on 21 August, whose thermogram was dominated by black carbon which represents the atmospheric carbonaceous component with lowest volatility and highest refractoriness, and was clearly distinct from all other air mass types which only contain a very minor BC fraction.

https://doi.org/10.5194/egusphere-2026-6814
Preprint. Discussion started: 12 November 2026
© Author(s) 2026. CC BY 4.0 License.

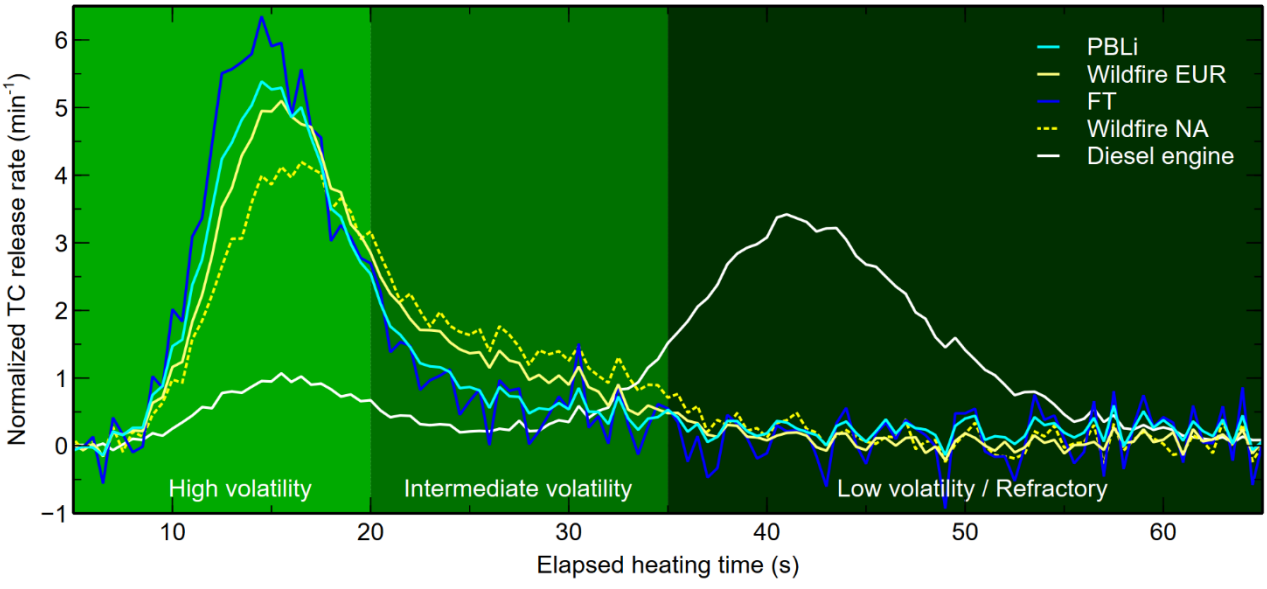


Figure 6: Average FATCAT thermograms: mean normalized carbon release rates (expressed per unit TC) as a function of elapsed heating time (a proxy for filter temperature, from ambient to ~800 °C) for five air mass categories including the local fossil fuel contamination event. The shaded regions delimit operationally defined volatility classes based on the temporal evolution of the carbon release signal: high volatility (0–20 s), intermediate volatility (20–35 s), and low volatility/refractory material (>35 s).

It can be noted that the wildfire plumes showed a lower volatility than PBLi and FT conditions, with carbon release extending into the intermediate volatility region (20–35 s heating time), beyond the high-volatility peak (<20 s) characteristic of the FT and PBLi air masses (Fig. 6). This is consistent with the heterogeneous composition of long-range-transported wildfire plumes, which combine primary biomass-burning emissions with aged organic material, spanning a wider range of thermal stabilities than either component alone (Keller et al., 2023). The observation of low-volatility and extremely low volatility organic matter in aged wildfire plumes is also consistent with previous studies (Lee et al., 2016; Paciga et al., 2016) and was observed in SOA produced from major organic gases emitted by biomass burning (Yu et al., 2016).

The FATCAT thermograms present a promising method for semi-quantitative distinction OC and EC, and for providing auxiliary data that may carry information on aerosol sources, such as combustion engines without particle filter (main fraction expected in refractory) versus wood burning (dominant fraction expected in intermediate to low volatility range), when taking measurements in close proximity of the emissions.

https://doi.org/10.5194/egusphere-2026-6814
Preprint. Discussion started: 12 November 2026
© Author(s) 2026. CC BY 4.0 License.

3.4.2. Volatility distribution of particulate organic carbon

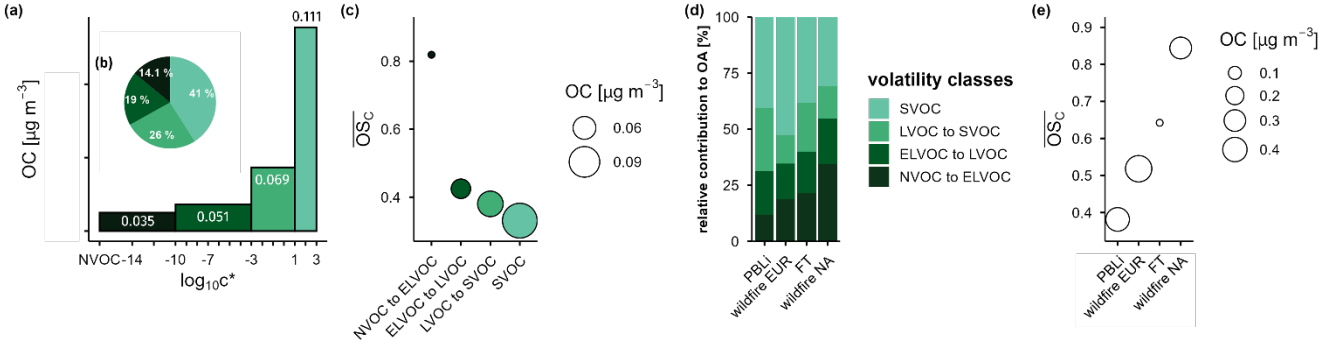


Figure 7: Volatility and oxidation state of the particulate organic carbon (pOC) overall and for the different air masses (*C calculated at 298.15 K). (a) Volatility distribution of pOC averaged across the whole campaign period. The area is proportional to the OC concentration, which is displayed in each bar. (b) This inset presents relative composition in terms of volatility classes indicated in the legend (c) Average carbon oxidation state (OSc) for the different volatility classes. (d) Relative contribution of the different volatility classes to OA for the different air mass types. (e) Carbon oxidation state for pOC for the different air mass types.**

The volatility distribution of carbonaceous matter governs its partitioning between gas and particle phase under given conditions. For this reason, volatility distributions of particulate organic carbon (pOC) were measured by putting a thermodenuder in front of an ACSM (see Section 2.2.5). Figure 7 presents the volatility distribution of pOC averaged over the whole campaign, as well as the relative contribution to pOC of the different volatility classes (panels a. and b.). Concentration-weighted campaign average carbon oxidation state (OSc) for the different volatility classes, calculated from the thermodenuder temperatures (Section 2.2.5), is given on Fig. 7c. The volatility classes are non-volatile to extremely low volatile OC (NVOC to ELVOC), ELVOC to low volatile OC (LVOC), LVOC to semi-volatile OC (SVOC), and SVOC. Aging of OA typically produces more oxidized compounds with reduced volatility due to polar functional groups. However, the volatility also depends on molecule size, as aging might fragment long-chain compounds, which would increase their volatility. Here, we observe that lower volatility classes had higher oxidation state. This suggests that OSc might be used as a proxy to have information on OA volatility when these measurements are not available. Despite the general high oxidation state of pOC, there was a substantial fraction of pOC in the highest volatility bin (SVOC) which, depending on the ambient conditions, could partition in the gas phase. It should be noted that this bin has the highest uncertainty as it was derived from a combination of both ACSMs.

Figure 7d. and e. show, for the different air masses, the relative contribution of the volatility classes to OA and the concentration-weighed carbon oxidation state, respectively. The volatility of OA is also presented on Fig. S20. As expected, PBLi OA showed more volatile, less oxidized OA than free troposphere conditions, due to having spent less time in the atmosphere. The North American wildfire organic aerosol was less volatile and more oxidized than the European plume, consistent with the longer estimated transport time (approximately 10 versus 1.6 days). However, differences in source composition, mixing, dilution and removal may also contribute, so the observed contrast cannot be attributed uniquely to atmospheric age. Both wildfire plumes OA were less volatile and more oxidized than PBLi conditions, on average.

https://doi.org/10.5194/egusphere-2026-6814
Preprint. Discussion started: 12 November 2026
© Author(s) 2026. CC BY 4.0 License.

Interestingly, FT OA was more volatile and less oxidized than the North American wildfire aerosol, potentially related to its different chemical composition.

3.4.3. Volatility of gaseous and particulate organic carbon

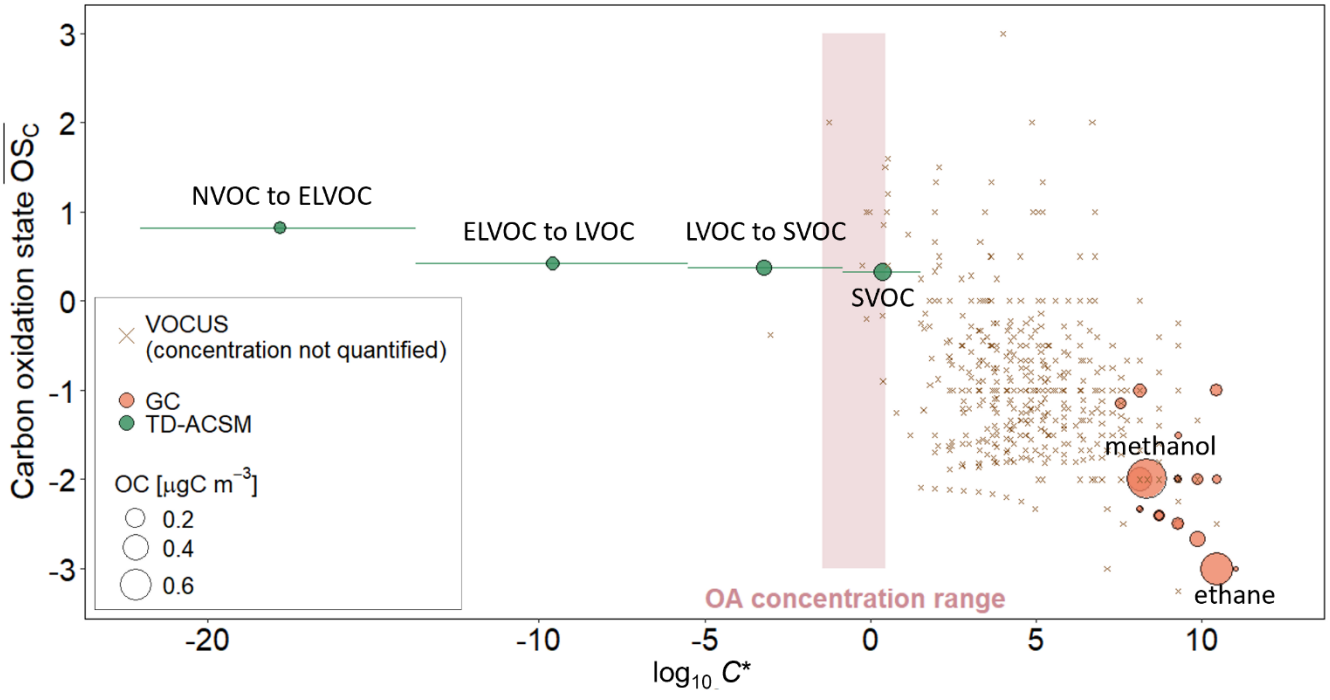


Figure 8: Carbon oxidation state (OSc) vs volatility ($\log_{10} C^*$) for organic carbon measured in both gas and particle phase by the GCs, the Vocus and the TD-ACSM at 273 K. The data from the GCs and the ACSM are quantitative in terms of OC concentration, while the Vocus is only qualitative. The names of the 2 VOCs with the highest concentration are indicated, as well as the TD-ACSM volatility classes. TD-ACSM volatility classes ranges are indicated by green segments. The ambient OA concentration range measured for this campaign is indicated on the figure.

Solving the phase partitioning of organic carbon between gas and particle phase requires knowledge of the overall volatility distribution considering both phases. Thus, the volatility of pOC introduced in the previous section was complemented by the volatility of the organic traces gases (CTGs) to obtain an overview of volatility and oxidation state as presented in Figure 8. Note the limitations of the data with the quantified CTGs being a subset of all gas-phase organic carbon, and the Vocus data not being quantitative in terms of carbon concentration. For the TD-ACSM data, the averaged $\log_{10} C^*$ values are presented as circles and the range of the volatility classes as error bars. Note that the saturation mass concentrations ($\log_{10} C^*$ values) were retrieved from direct measurements for pOC while they were calculated based on the molecular formulas of the compounds or fragments detected by the Vocus and the GCs, which can lead to discrepancies. The C^* values (µg m^{-3}) of the CTGs were calculated initially at 300 K, as per Donahue et al. (2011), then converted to 273 K (see Eq. 7) to be more representative of ambient temperatures at JFJ. For the TD-ACSM, they were measured at laboratory temperature (~298 K) and converted to

https://doi.org/10.5194/egusphere-2026-6814
Preprint. Discussion started: 12 November 2026
© Author(s) 2026. CC BY 4.0 License.

273.15 K as well (Eq. 7). The graph at measured or calculated temperatures is presented on Fig. S21, where the points are shifted to higher volatility compared to Figure 8, as expected. Average carbon oxidation states (OSc) were calculated to present the data in a 2D-volatility basis set (Donahue et al., 2011). They were calculated based on *f*43 and *f*44 for the TD-ACSM data (see Section 2.2.4) and based on the molecular formulas for the Vocus and the GCs. Note that the PTR-MS technique using H_3O^+ as a reagent ions is limited in terms of capturing compounds with volatilities lower than IVOCs. For such compounds, other techniques such as Iodide-CIMS would be more suitable.

Despite these limitations, Fig. 8 shows that organic carbon at JFJ covers a wide range of volatilities. The most volatile pOC and the least volatile VOCs overlap in terms of *C**. Such overlap is expected based on Donahue's equation for equilibrium phase partitioning (Donahue et al., 2012), which predicts that the transition from 10% to 90% in the gas phase happens across two orders in magnitude of *C**. More so, this overlap of pOC and VOCs ranges occurs around *C**-values equal to observed particulate organic mass concentrations (red shading in Fig. 8), again consistent with Donahue's equation. This gives confidence on the volatility distribution quantified with a combination of different methods. The fact that a substantial fraction of OC, compared to total pOC levels, falls into the semi-volatility range overlapping with observed OA concentrations implies that the organic aerosol is sensitive to repartitioning between gas and particle phase if conditions change, e.g. change in temperature, humidity or OA mass concentration. The general relationship of decreasing carbon oxidation state with increasing volatility was maintained from pOC through to VOCs, and the highest OC concentrations were detected in the gas phase with OSc smaller than around -2.

Compared to Hunter et al. (2017), the concentrations obtained at JFJ were lower, especially in the gas phase, due to the lack of measurements of compounds such as acetone and IVOCs in our study, due to the site being remote and because our results were not corrected for standard conditions. However, thanks to the GC measurements, we extended to lower carbon oxidation states with alkanes such as ethane, that have relatively high OC concentrations. But despite the different techniques used, the results are fairly comparable.

https://doi.org/10.5194/egusphere-2026-6814
Preprint. Discussion started: 12 November 2026
© Author(s) 2026. CC BY 4.0 License.

4 Conclusions

This study characterized gas- and particle-phase atmospheric carbon at Jungfraujoch, Switzerland (3580 m a.s.l.), using a comprehensive suite of instruments deployed from 16 August to 20 September 2022. The PM_1 concentration was 0.98 µg m^{-3} on average and mostly below 5 µg m^{-3} and was dominated by organic aerosol. Despite experimental issues faced with the gas-phase measurements, 66 carbonaceous trace gases (CTG) could be quantified using 2 GCs, which presents only a fraction of total gaseous trace carbon. The total quantified CTG concentration was 2.3 µg C m^{-3} on average but stayed mostly above 1 µgC m^{-3} because of the long-lived species it includes (halogenated compounds, COS). The two highest compounds were methanol and ethane.

Particulate OC volatility measurements were performed using a thermo-denuder upstream of the ACSM and resolved four volatility classes. Combining these measurements with calculated volatilities for gas-phase OC provided an overview of the total volatility range at JFJ, with the 2D-volatility basis set ranging from oxidation states -3.25 to 3 and volatility (as $\log10_{\text{eff}}\, C^*$) ranging from -22 to 11.1. A substantial fraction of OC was in the semi-volatile range and fell in the volatility range overlapping with ambient OA concentrations, which implies that it is sensitive to repartitioning between gas and particle phase, depending on ambient conditions.

During the campaign, JFJ was 23% of the time in free tropospheric (FT) conditions and influenced by planetary boundary layer intrusions (PBLi), as well as a Saharan dust event and two wildfire episodes. The concentrations of both particulate matter and carbonaceous trace gases increased for PBLi compared to free tropospheric conditions. The contribution of alcohols increased for PBLi, while the contribution of halogenated compounds and alkanes increased in free tropospheric conditions, due to their longer lifetimes. The wildfires also impacted both PM_1 and CTGs, their concentrations increased during the wildfire from Europe, and their composition changed for both wildfires, with more organic aerosol (OA) for the one from North America (79% on average) and more alcohols for the one from Europe (56% on average). The wildfires also changed the composition of OA, with increased fractions of fragments with high m/z (≥ 135), and its volatility, with less volatile pOC during the wildfires, especially the one from North America.

Local emissions from touristic activities, which have previously been reported for particulate matter, were also observed for volatile organic compounds (VOCs), which were measured, but not quantified, by a Vocus PTR-MS. A fraction of the 403 ions detected could be attributed to PBLi, while a specific cluster likely originated from touristic activities, in particular cooking emissions from the local restaurant and volatile chemical products. The total VOC contribution, especially IVOCs, to the overall gaseous carbon thus remains uncertain and needs further studies.

A complete mass closure for total atmospheric carbon could not be obtained due to the lack of measurements in the gas phase. Total particulate carbon was obtained by four independent techniques and showed reasonable agreement (R^2 = 0.89-0.98, factor 1.06-2.69).

https://doi.org/10.5194/egusphere-2026-6814
Preprint. Discussion started: 12 November 2026
© Author(s) 2026. CC BY 4.0 License.

The CBC campaign provided the first measurement series in which FATCAT thermograms were systematically examined across contrasting air mass types, and the results support their semi-quantitative interpretation in terms of aerosol volatility and refractoriness. These measurements showed a lower volatility for total carbon during the wildfire plumes than FT and PBL conditions.

This work contributes to a better understanding of free tropospheric carbonaceous compounds, as these are harder to study due to the local constraints. Such high-altitude remote location is expected to be rather clean. However, in a changing climate and with an increasing impact of wildfires in the Northern hemisphere, the oxidation state and volatility of aerosol in the high altitude might be more impacted, with potential effects on the climate. Future work at other high-altitude stations would help assessing these impacts more globally.

Data and code availability

The ACTRIS data is available at https://ebas.nilu.no. Data is available from the corresponding authors upon request.

Author contributions

LS: Investigation, Visualization, Writing (original draft preparation); NN: Formal analysis, Investigation, Visualization, Writing (review and editing); SJA: Investigation, Resources; MB: Investigation, Writing (review & editing); DB: Methodology, Investigation, Writing (review & editing); BTB: Conceptualization, Investigation, Supervision, Writing (review and editing); FC: Investigation, Resources; RKYC: Investigation; ZCJD: Investigation, Writing (review & editing); JRH: Investigation, Resources; CH: Investigation, Resources; MI: Investigation, Resources; AK: Investigation, Resources, Visualization, Writing (review and editing); GL: Investigation, Resources; TL: Investigation, Resources; RM: Investigation, Supervision, Writing (review and editing); JPP: Investigation, Resources; SR: Investigation, Resources; MR: Investigation, Resources, Writing (review and editing); TS: Investigation, Resources; MS: Investigation, Resources; MKV: Investigation, Resources, Writing (review and editing); EW: Investigation, Resources, MGB: Conceptualization, Investigation, Funding acquisition, Resources Supervision, Writing (review and editing)

Competing interests

AK and EW are affiliated with the University of Applied Sciences and Arts Northwestern Switzerland (FHNW), where the FATCAT instrument was designed and built. FATCAT is not a commercial product, and FHNW has no financial interest in it. At the time of the research, MR was employed by the manufacturer of the Aethalometer and TCA08 instruments.

https://doi.org/10.5194/egusphere-2026-6814
Preprint. Discussion started: 12 November 2026
© Author(s) 2026. CC BY 4.0 License.

Acknowledgements

We would like to thank the International Foundation High Altitude Research Stations Jungfraujoch and Gornergrat (HFSJG), 3012 Bern, Switzerland, and its staff team for enabling us to carry out our experiments at the Jungfraujoch High Altitude Research Station.We also acknowledge Pascal Schneider, Levi Folghera and the HFSJG custodians for technical support at Jungfraujoch. We thank the Federal Office of Meteorology and Climatology MeteoSwiss for the provision of meteorological data. We also thank Franz Conen (University of Basel) for the operation of the Radon analyzer. This work has been supported by the ACTRIS IMP (TransNational Access Programme) funded by the European Commission under the Horizon 2020 – Research and Innovation Framework Programme, H2020-INFRADEV-2019-2, Grant Agreement number: 871115. The authors wish to acknowledge the ACTRIS (Aerosol, Clouds, and Trace Gases Research Infrastructure) for its essential role in providing access to high-quality data, facilities, and technical support, here from CiGas, that were integral to the execution of this research. Generative AI was used in this work to improve the wording of a few sentences. The authors reviewed and edited the content as needed and take full responsibility for the content of the publication.

Financial Support

This activity also received financial support through the TNA scheme of ACTRIS IMP project funded by the European Commission under Horizon 2020 – Research and Innovation Framework Programme, H2020-INFRADEV-2019-2, Grant Agreement number: 871115. Continuous aerosol observations at the Jungfraujoch received financial support through the ACTRIS Switzerland 2025-2028 grant (Swiss contribution to the ACTRIS ERIC) funded by the Swiss State Secretariat for Education and Research and Innovation (SERI) from MeteoSwiss in the framework of the Global Atmosphere Watch (GAW) program of the World Meteorological Organization (WMO).

Support for the Medusa-GCMS measurements was provided by the Swiss National Programs HALCLIM and CLIMGAS-CH (Swiss Federal Office for the Environment, FOEN). The International Foundation High Altitude Research Stations Jungfraujoch and Gornergrat is generously supported by the Swiss National Science Foundation (SNSF) (grant No. 20FI-0_238048). ^{222}Rn measurements at Jungfraujoch were supported by ICOS-CH (Swiss National Science Foundation, grant 20FI20_198227). TS and TL participation was supported by ACTRIS IMP (TransNational Access Programme) of the European Commission: grant agreement No 871115.

References

Affolter, S., Schibig, M., Berhanu, T., Bukowiecki, N., Steinbacher, M., Nyfeler, P., Hervo, M., Lauper, J., Leuenberger, M., 2021. Assessing local CO_2 contamination revealed by two near-by high altitude records at Jungfraujoch, Switzerland. Environ. Res. Lett. 16, 044037. https://doi.org/10.1088/1748-9326/abe74a

Anderson, T.L., Ogren, J.A., 1998. Determining Aerosol Radiative Properties Using the TSI 3563 Integrating Nephelometer. Aerosol Science and Technology 29, 57–69. https://doi.org/10.1080/02786829808965551

https://doi.org/10.5194/egusphere-2026-6814
Preprint. Discussion started: 12 November 2026
© Author(s) 2026. CC BY 4.0 License.

Appenzeller, C., Begert, M., Zenklusen, E., Scherrer, S.C., 2008. Monitoring climate at Jungfraujoch in the high Swiss Alpine region. Science of The Total Environment 391, 262–268. https://doi.org/10.1016/j.scitotenv.2007.10.005

Atkinson, R., 2000. Atmospheric chemistry of VOCs and NOx. Atmospheric Environment 34, 2063–2101. https://doi.org/10.1016/S1352-2310(99)00460-4

Aydin, M., Williams, M.B., Tatum, C., Saltzman, E.S., 2008. Carbonyl sulfide in air extracted from a South Pole ice core: a 2000 year record. Atmos. Chem. Phys. https://doi.org/10.5194/acp-8-7533-2008

Baumgardner, D., Popovicheva, O., Allan, J., Bernardoni, V., Cao, J., Cavalli, F., Cozic, J., Diapouli, E., Eleftheriadis, K., Genberg, P.J., Gonzalez, C., Gysel, M., John, A., Kirchstetter, T.W., Kuhlbusch, T.A.J., Laborde, M., Lack, D., Müller, T., Niessner, R., Petzold, A., Piazzalunga, A., Putaud, J.P., Schwarz, J., Sheridan, P., Subramanian, R., Swietlicki, E., Valli, G., Vecchi, R., Viana, M., 2012. Soot reference materials for instrument calibration and intercomparisons: a workshop summary with recommendations. Atmos. Meas. Tech. 5, 1869–1887. https://doi.org/10.5194/amt-5-1869-2012

Bond, T.C., Doherty, S.J., Fahey, D.W., Forster, P.M., Berntsen, T., DeAngelo, B.J., Flanner, M.G., Ghan, S., Kärcher, B., Koch, D., Kinne, S., Kondo, Y., Quinn, P.K., Sarofim, M.C., Schultz, M.G., Schulz, M., Venkataraman, C., Zhang, H., Zhang, S., Bellouin, N., Guttikunda, S.K., Hopke, P.K., Jacobson, M.Z., Kaiser, J.W., Klimont, Z., Lohmann, U., Schwarz, J.P., Shindell, D., Storelvmo, T., Warren, S.G., Zender, C.S., 2013. Bounding the role of black carbon in the climate system: A scientific assessment. JGR Atmospheres 118, 5380–5552. https://doi.org/10.1002/jgrd.50171

Brunner, C., Brem, B.T., Collaud Coen, M., Conen, F., Hervo, M., Henne, S., Steinbacher, M., Gysel-Beer, M., Kanji, Z.A., 2021. The contribution of Saharan dust to the ice-nucleating particle concentrations at the High Altitude Station Jungfraujoch (3580 m a.s.l.), Switzerland. Atmos. Chem. Phys. 21, 18029–18053. https://doi.org/10.5194/acp-21-18029-2021

Bukowiecki, N., Brem, B.T., Wehrle, G., Močnik, G., Affolter, S., Leuenberger, M., Coen, M.C., Hervo, M., Baltensperger, U., Gysel-Beer, M., 2021. Elucidating local pollution and site representativeness at the Jungfraujoch, Switzerland through parallel aerosol measurements at an adjacent mountain ridge. Environ. Res. Commun. 3, 021001. https://doi.org/10.1088/2515-7620/abe987

Bukowiecki, N., Weingartner, E., Gysel, M., Coen, M.C., Zieger, P., Herrmann, E., Steinbacher, M., Ga¨ggeler, H.W., Baltensperger, U., 2016. A Review of More than 20 Years of Aerosol Observation at the High Altitude Research Station Jungfraujoch, Switzerland (3580 m asl). Aerosol Air Qual. Res. 16, 764–788. https://doi.org/10.4209/aaqr.2015.05.0305

Canagaratna, M.R., Jimenez, J.L., Kroll, J.H., Chen, Q., Kessler, S.H., Massoli, P., Hildebrandt Ruiz, L., Fortner, E., Williams, L.R., Wilson, K.R., Surratt, J.D., Donahue, N.M., Jayne, J.T., Worsnop, D.R., 2015. Elemental ratio measurements of organic compounds using aerosol mass spectrometry: characterization, improved calibration, and implications. Atmos. Chem. Phys. 15, 253–272. https://doi.org/10.5194/acp-15-253-2015

Coggon, M.M., Stockwell, C.E., Xu, L., Peischl, J., Gilman, J.B., Lamplugh, A., Bowman, H.J., Aikin, K., Harkins, C., Zhu, Q., Schwantes, R.H., He, J., Li, M., Seltzer, K., McDonald, B., Warneke, C., 2024. Contribution of cooking emissions to the urban volatile organic compounds in Las Vegas, NV. Atmos. Chem. Phys. 24, 4289–4304. https://doi.org/10.5194/acp-24-4289-2024

Collaud Coen, M., Brem, B.T., Gysel-Beer, M., Modini, R., Henne, S., Steinbacher, M., Putero, D., Gini, M.I., Eleftheriadis, K., 2026. Detection and climatology of Saharan dust frequency and mass at the Jungfraujoch (3580 m a.s.l., Switzerland). Atmos. Chem. Phys. 26, 1623–1645. https://doi.org/10.5194/acp-26-1623-2026

Collaud Coen, M., Weingartner, E., Furger, M., Nyeki, S., Prévôt, A.S.H., Steinbacher, M., Baltensperger, U., 2011. Aerosol climatology and planetary boundary influence at the Jungfraujoch analyzed by synoptic weather types. Atmos. Chem. Phys. 11, 5931–5944. https://doi.org/10.5194/acp-11-5931-2011

Collaud Coen, M., Weingartner, E., Schaub, D., Hueglin, C., Corrigan, C., Henning, S., Schwikowski, M., Baltensperger, U., 2004. Saharan dust events at the Jungfraujoch: detection by wavelength dependence of the single scattering albedo and first climatology analysis. Atmos. Chem. Phys. 4, 2465–2480. https://doi.org/10.5194/acp-4-2465-2004

Corbin, J.C., Clavel, D., Smallwood, G.J., 2024. Characterization of two aerosol carbon analyzers based on temperature programmed oxidation: TCA08 and FATCAT. Aerosol Science and Technology 58, 812–829. https://doi.org/10.1080/02786826.2024.2351991

https://doi.org/10.5194/egusphere-2026-6814
Preprint. Discussion started: 12 November 2026
© Author(s) 2026. CC BY 4.0 License.

Cozic, J., Verheggen, B., Weingartner, E., Crosier, J., Bower, K.N., Flynn, M., Coe, H., Henning, S., Steinbacher, M., Henne, S., Coen, M.C., Petzold, A., Baltensperger, U., 2008. Chemical composition of free tropospheric aerosol for PM1 and coarse mode at the high alpine site Jungfraujoch. Atmos. Chem. Phys. https://doi.org/10.5194/acp-8-407-2008

Donahue, N.M., Epstein, S.A., Pandis, S.N., Robinson, A.L., 2011. A two-dimensional volatility basis set: 1. organic-aerosol mixing thermodynamics. Atmos. Chem. Phys. 11, 3303–3318. https://doi.org/10.5194/acp-11-3303-2011

Donahue, N.M., Kroll, J.H., Pandis, S.N., Robinson, A.L., 2012. A two-dimensional volatility basis set – Part 2: Diagnostics of organic-aerosol evolution. Atmos. Chem. Phys. 12, 615–634. https://doi.org/10.5194/acp-12-615-2012

Empa, 2025. Technischer Bericht zum Nationalen Beobachtungsnetz für Luftfremdstoffe (NABEL) 2025. https://www.empa.ch/documents/d/s503/technischer-bericht-nabel-2025

Epstein, S.A., Riipinen, I., Donahue, N.M., 2010. A Semiempirical Correlation between Enthalpy of Vaporization and Saturation Concentration for Organic Aerosol. Environ. Sci. Technol. 44, 743–748. https://doi.org/10.1021/es902497z

Favez, O., Gherras, M., Müller, T., Wiedensohler, A., Fiebig, M, Eckhart, P., Savadkoohi, M., Pandolfi, M., 2024. Report guidance to produce eBC concentrations from NRT ACTRIS absorption measurements. https://www.actris-ecac.eu/files/ACTRISforCAMS_eBC_level3_data_product_guidance.pdf

Fischer, H., Nikitas, C., Parchatka, U., Zenker, T., Harris, G.W., Matuska, P., Schmitt, R., Mihelcic, D., Muesgen, P., Paetz, H. -W., Schultz, M., Volz-Thomas, A., 1998. Trace gas measurements during the Oxidizing Capacity of the Tropospheric Atmosphere campaign 1993 at Izaña. J. Geophys. Res. 103, 13505–13518. https://doi.org/10.1029/97JD01497

Fröhlich, R., Cubison, M.J., Slowik, J.G., Bukowiecki, N., Canonaco, F., Croteau, P.L., Gysel, M., Henne, S., Herrmann, E., Jayne, J.T., Steinbacher, M., Worsnop, D.R., Baltensperger, U., Prévôt, A.S.H., 2015. Fourteen months of on-line measurements of the non-refractory submicron aerosol at the Jungfraujoch (3580 m a.s.l.) – chemical composition, origins and organic aerosol sources. Atmos. Chem. Phys. 15, 11373–11398. https://doi.org/10.5194/acp-15-11373-2015

Fröhlich, R., Cubison, M.J., Slowik, J.G., Bukowiecki, N., Prévôt, A.S.H., Baltensperger, U., Schneider, J., Kimmel, J.R., Gonin, M., Rohner, U., Worsnop, D.R., Jayne, J.T., 2013. The ToF-ACSM: a portable aerosol chemical speciation monitor with TOFMS detection. Atmos. Meas. Tech. 6, 3225–3241. https://doi.org/10.5194/amt-6-3225-2013

Garofalo, L.A., Pothier, M.A., Levin, E.J.T., Campos, T., Kreidenweis, S.M., Farmer, D.K., 2019. Emission and Evolution of Submicron Organic Aerosol in Smoke from Wildfires in the Western United States. ACS Earth Space Chem. 3, 1237–1247. https://doi.org/10.1021/acsearthspacechem.9b00125

Giglio, L., Randerson, J.T., Van Der Werf, G.R., 2013. Analysis of daily, monthly, and annual burned area using the fourth-generation global fire emissions database (GFED4). JGR Biogeosciences 118, 317–328. https://doi.org/10.1002/jgrg.20042

Griffiths, A.D., Conen, F., Weingartner, E., Zimmermann, L., Chambers, S.D., Williams, A.G., Steinbacher, M., 2014. Surface-to-mountaintop transport characterised by radon observations at the Jungfraujoch. Atmos. Chem. Phys. 14, 12763–12779. https://doi.org/10.5194/acp-14-12763-2014

Gysel, M., Laborde, M., Olfert, J.S., Subramanian, R., Gröhn, A.J., 2011. Effective density of Aquadag and fullerene soot black carbon reference materials used for SP2 calibration. Atmos. Meas. Tech. 4, 2851–2858. https://doi.org/10.5194/amt-4-2851-2011

Heiskanen, J., Brümmer, C., Buchmann, N., Calfapietra, C., Chen, H., Gielen, B., Gkritzalis, T., Hammer, S., Hartman, S., Herbst, M., Janssens, I.A., Jordan, A., Juurola, E., Karstens, U., Kasurinen, V., Kruijt, B., Lankreijer, H., Levin, I., Linderson, M.-L., Loustau, D., Merbold, L., Myhre, C.L., Papale, D., Pavelka, M., Pilegaard, K., Ramonet, M., Rebmann, C., Rinne, J., Rivier, L., Saltikoff, E., Sanders, R., Steinbacher, M., Steinhoff, T., Watson, A., Vermeulen, A.T., Vesala, T., Vítková, G., Kutsch, W., 2022. The Integrated Carbon Observation System in Europe. Bulletin of the American Meteorological Society 103, E855–E872. https://doi.org/10.1175/BAMS-D-19-0364.1

Herrmann, E., Weingartner, E., Henne, S., Vuilleumier, L., Bukowiecki, N., Steinbacher, M., Conen, F., Collaud Coen, M., Hammer, E., Jurányi, Z., Baltensperger, U., Gysel, M., 2015. Analysis of long-term aerosol size distribution data from Jungfraujoch with emphasis on free tropospheric conditions, cloud influence, and air mass transport. JGR Atmospheres 120, 9459–9480. https://doi.org/10.1002/2015JD023660

https://doi.org/10.5194/egusphere-2026-6814
Preprint. Discussion started: 12 November 2026
© Author(s) 2026. CC BY 4.0 License.

Hunter, J.F., Day, D.A., Palm, B.B., Yatavelli, R.L.N., Chan, A.W.H., Kaser, L., Cappellin, L., Hayes, P.L., Cross, E.S., Carrasquillo, A.J., Campuzano-Jost, P., Stark, H., Zhao, Y., Hohaus, T., Smith, J.N., Hansel, A., Karl, T., Goldstein, A.H., Guenther, A., Worsnop, D.R., Thornton, J.A., Heald, C.L., Jimenez, J.L., Kroll, J.H., 2017. Comprehensive characterization of atmospheric organic carbon at a forested site. Nature Geosci 10, 748–753. https://doi.org/10.1038/ngeo3018

Isaacman-VanWertz, G., Massoli, P., O'Brien, R., Lim, C., Franklin, J.P., Moss, J.A., Hunter, J.F., Nowak, J.B., Canagaratna, M.R., Misztal, P.K., Arata, C., Roscioli, J.R., Herndon, S.T., Onasch, T.B., Lambe, A.T., Jayne, J.T., Su, L., Knopf, D.A., Goldstein, A.H., Worsnop, D.R., Kroll, J.H., 2018. Chemical evolution of atmospheric organic carbon over multiple generations of oxidation. Nature Chem 10, 462–468. https://doi.org/10.1038/s41557-018-0002-2

Isaacman-VanWertz, G., Massoli, P., O'Brien, R.E., Nowak, J.B., Canagaratna, M.R., Jayne, J.T., Worsnop, D.R., Su, L., Knopf, D.A., Misztal, P.K., Arata, C., Goldstein, A.H., Kroll, J.H., 2017. Using advanced mass spectrometry techniques to fully characterize atmospheric organic carbon: current capabilities and remaining gaps. Faraday Discuss. 200, 579–598. https://doi.org/10.1039/C7FD00021A

Jobson, B.T., McKeen, S.A., Parrish, D.D., Fehsenfeld, F.C., Blake, D.R., Goldstein, A.H., Schauffler, S.M., Elkins, J.W., 1999. Trace gas mixing ratio variability versus lifetime in the troposphere and stratosphere: Observations. J. Geophys. Res. 104, 16091–16113. https://doi.org/10.1029/1999JD900126

Jurányi, Z., Gysel, M., Weingartner, E., DeCarlo, P.F., Kammermann, L., Baltensperger, U., 2010. Measured and modelled cloud condensation nuclei number concentration at the high alpine site Jungfraujoch. Atmos. Chem. Phys. 10, 7891–7906. https://doi.org/10.5194/acp-10-7891-2010

Keller, A., Burtscher, H., Weingartner, E., 2026. Swiss Made Measurement Techniques for Carbonaceous Aerosols. Chimia 80, 21–28. https://doi.org/10.2533/chimia.2026.21

Keller, A., Specht, P., Steigmeier, P., Weingartner, E., 2023. A novel measurement system for unattended, in situ characterization of carbonaceous aerosols. Aerosol Research 1, 65–79. https://doi.org/10.5194/ar-1-65-2023

Klein, F., Platt, S.M., Farren, N.J., Detournay, A., Bruns, E.A., Bozzetti, C., Daellenbach, K.R., Kilic, D., Kumar, N.K., Pieber, S.M., Slowik, J.G., Temime-Roussel, B., Marchand, N., Hamilton, J.F., Baltensperger, U., Prévôt, A.S.H., El Haddad, I., 2016. Characterization of Gas-Phase Organics Using Proton Transfer Reaction Time-of-Flight Mass Spectrometry: Cooking Emissions. Environ. Sci. Technol. 50, 1243–1250. https://doi.org/10.1021/acs.est.5b04618

Krechmer, J., Lopez-Hilfiker, F., Koss, A., Hutterli, M., Stoermer, C., Deming, B., Kimmel, J., Warneke, C., Holzinger, R., Jayne, J., Worsnop, D., Fuhrer, K., Gonin, M., De Gouw, J., 2018. Evaluation of a New Reagent-Ion Source and Focusing Ion–Molecule Reactor for Use in Proton-Transfer-Reaction Mass Spectrometry. Anal. Chem. 90, 12011–12018. https://doi.org/10.1021/acs.analchem.8b02641

Krivácsy, Z., Hoffer, A., Sárvári, Zs., Temesi, D., Baltensperger, U., Nyeki, S., Weingartner, E., Kleefeld, S., Jennings, S.G., 2001. Role of organic and black carbon in the chemical composition of atmospheric aerosol at European background sites. Atmospheric Environment 35, 6231–6244. https://doi.org/10.1016/S1352-2310(01)00467-8

Kroll, J.H., Smith, J.D., Che, D.L., Kessler, S.H., Worsnop, D.R., Wilson, K.R., 2009. Measurement of fragmentation and functionalization pathways in the heterogeneous oxidation of oxidized organic aerosol. Phys. Chem. Chem. Phys. 11, 8005. https://doi.org/10.1039/b905289e

Laborde, M., Mertes, P., Zieger, P., Dommen, J., Baltensperger, U., Gysel, M., 2012. Sensitivity of the Single Particle Soot Photometer to different black carbon types. Atmos. Meas. Tech. 5, 1031–1043. https://doi.org/10.5194/amt-5-1031-2012

Lanz, V.A., Henne, S., Staehelin, J., Hueglin, C., Vollmer, M.K., Steinbacher, M., Buchmann, B., Reimann, S., 2009. Statistical analysis of anthropogenic non-methane VOC variability at a European background location (Jungfraujoch, Switzerland). Atmos. Chem. Phys. 9, 3445–3459. https://doi.org/10.5194/acp-9-3445-2009

Lanz, V.A., Prévôt, A.S.H., Alfarra, M.R., Weimer, S., Mohr, C., DeCarlo, P.F., Gianini, M.F.D., Hueglin, C., Schneider, J., Favez, O., D'Anna, B., George, C., Baltensperger, U., 2010. Characterization of aerosol chemical composition with aerosol mass spectrometry in Central Europe: an overview. Atmos. Chem. Phys. 10, 10453–10471. https://doi.org/10.5194/acp-10-10453-2010

Lee, A.K.Y., Willis, M.D., Healy, R.M., Wang, J.M., Jeong, C.-H., Wenger, J.C., Evans, G.J., Abbatt, J.P.D., 2016. Single-particle characterization of biomass burning organic aerosol (BBOA): evidence for non-uniform mixing of high

https://doi.org/10.5194/egusphere-2026-6814
Preprint. Discussion started: 12 November 2026
© Author(s) 2026. CC BY 4.0 License.

molecular weight organics and potassium. Atmos. Chem. Phys. 16, 5561–5572. https://doi.org/10.5194/acp-16-5561-2016

Legreid, G., Folini, D., Staehelin, J., Lööv, J.B., Steinbacher, M., Reimann, S., 2008. Measurements of organic trace gases including oxygenated volatile organic compounds at the high alpine site Jungfraujoch (Switzerland): Seasonal variation and source allocations. Journal of Geophysical Research: Atmospheres 113, 5307. https://doi.org/10.1029/2007JD008653

Li, Y., Pöschl, U., Shiraiwa, M., 2016. Molecular corridors and parameterizations of volatility in the chemical evolution of organic aerosols. Atmos. Chem. Phys. 16, 3327–3344. https://doi.org/10.5194/acp-16-3327-2016

Mohr, C., Gysel-Beer, M., 2024. The Chemistry of Atmospheric Aerosols: At the Nexus Between Climate, Energy, and Air Quality. Chimia 78, 728–733. https://doi.org/10.2533/chimia.2024.728

Montzka, S.A., Calvert, P., Hall, B.D., Elkins, J.W., Conway, T.J., Tans, P.P., Sweeney, C., 2007. On the global distribution, seasonality, and budget of atmospheric carbonyl sulfide (COS) and some similarities to CO_2. J. Geophys. Res. 112, 2006JD007665. https://doi.org/10.1029/2006JD007665

Müller, T., Henzing, J.S., De Leeuw, G., Wiedensohler, A., Alastuey, A., Angelov, H., Bizjak, M., Collaud Coen, M., Engström, J.E., Gruening, C., Hillamo, R., Hoffer, A., Imre, K., Ivanow, P., Jennings, G., Sun, J.Y., Kalivitis, N., Karlsson, H., Komppula, M., Laj, P., Li, S.-M., Lunder, C., Marinoni, A., Martins Dos Santos, S., Moerman, M., Nowak, A., Ogren, J.A., Petzold, A., Pichon, J.M., Rodriquez, S., Sharma, S., Sheridan, P.J., Teinilä, K., Tuch, T., Viana, M., Virkkula, A., Weingartner, E., Wilhelm, R., Wang, Y.Q., 2011. Characterization and intercomparison of aerosol absorption photometers: result of two intercomparison workshops. Atmos. Meas. Tech. 4, 245–268. https://doi.org/10.5194/amt-4-245-2011

Ng, N.L., Herndon, S.C., Trimborn, A., Canagaratna, M.R., Croteau, P.L., Onasch, T.B., Sueper, D., Worsnop, D.R., Zhang, Q., Sun, Y.L., Jayne, J.T., 2011. An Aerosol Chemical Speciation Monitor (ACSM) for Routine Monitoring of the Composition and Mass Concentrations of Ambient Aerosol. Aerosol Science and Technology 45, 780–794. https://doi.org/10.1080/02786826.2011.560211

Ortiz-Amezcua, P., Guerrero-Rascado, J.L., Granados-Muñoz, M.J., Benavent-Oltra, J.A., Böckmann, C., Samaras, S., Stachlewska, I.S., Janicka, Ł., Baars, H., Bohlmann, S., Alados-Arboledas, L., 2017. Microphysical characterization of long-range transported biomass burning particles from North America at three EARLINET stations. Atmos. Chem. Phys. 17, 5931–5946. https://doi.org/10.5194/acp-17-5931-2017

Paciga, A., Karnezi, E., Kostenidou, E., Hildebrandt, L., Psichoudaki, M., Engelhart, G.J., Lee, B.-H., Crippa, M., Prévôt, A.S.H., Baltensperger, U., Pandis, S.N., 2016. Volatility of organic aerosol and its components in the megacity of Paris. Atmos. Chem. Phys. 16, 2013–2023. https://doi.org/10.5194/acp-16-2013-2016

Petzold, A., Ogren, J.A., Fiebig, M., Laj, P., Li, S.-M., Baltensperger, U., Holzer-Popp, T., Kinne, S., Pappalardo, G., Sugimoto, N., Wehrli, C., Wiedensohler, A., Zhang, X.-Y., 2013. Recommendations for reporting "black carbon" measurements. Atmos. Chem. Phys. 13, 8365–8379. https://doi.org/10.5194/acp-13-8365-2013

Prinn, R.G., Weiss, R.F., Arduini, J., Arnold, T., DeWitt, H.L., Fraser, P.J., Ganesan, A.L., Gasore, J., Harth, C.M., Hermansen, O., Kim, J., Krummel, P.B., Li, S., Loh, Z.M., Lunder, C.R., Maione, M., Manning, A.J., Miller, B.R., Mitrevski, B., Mühle, J., O'Doherty, S., Park, S., Reimann, S., Rigby, M., Saito, T., Salameh, P.K., Schmidt, R., Simmonds, P.G., Steele, L.P., Vollmer, M.K., Wang, R.H., Yao, B., Yokouchi, Y., Young, D., Zhou, L., 2018. History of chemically and radiatively important atmospheric gases from the Advanced Global Atmospheric Gases Experiment (AGAGE). Earth Syst. Sci. Data 10, 985–1018. https://doi.org/10.5194/essd-10-985-2018

Rigler, M., Drinovec, L., Lavrič, G., Vlachou, A., Prévôt, A.S.H., Jaffrezo, J.L., Stavroulas, I., Sciare, J., Burger, J., Kranjc, I., Turšič, J., Hansen, A.D.A., Močnik, G., 2020. The new instrument using a TC–BC (total carbon–black carbon) method for the online measurement of carbonaceous aerosols. Atmos. Meas. Tech. 13, 4333–4351. https://doi.org/10.5194/amt-13-4333-2020

Saha, P.K., Grieshop, A.P., 2016. Exploring Divergent Volatility Properties from Yield and Thermodenuder Measurements of Secondary Organic Aerosol from α-Pinene Ozonolysis. Environ. Sci. Technol. 50, 5740–5749. https://doi.org/10.1021/acs.est.6b00303

Samset, B.H., 2022. Aerosol absorption has an underappreciated role in historical precipitation change. Commun Earth Environ 3, 242. https://doi.org/10.1038/s43247-022-00576-6

© Author(s) 2026. CC BY 4.0 License.

Schwarz, J.P., Gao, R.S., Fahey, D.W., Thomson, D.S., Watts, L.A., Wilson, J.C., Reeves, J.M., Darbeheshti, M., Baumgardner, D.G., Kok, G.L., Chung, S.H., Schulz, M., Hendricks, J., Lauer, A., Kärcher, B., Slowik, J.G., Rosenlof, K.H., Thompson, T.L., Langford, A.O., Loewenstein, M., Aikin, K.C., 2006. Single-particle measurements of midlatitude black carbon and light-scattering aerosols from the boundary layer to the lower stratosphere. J. Geophys. Res. 111, 2006JD007076. https://doi.org/10.1029/2006JD007076

Sellegri, K., Laj, P., Peron, F., Dupuy, R., Legrand, M., Preunkert, S., Putaud, J. -P., Cachier, H., Ghermandi, G., 2003. Mass balance of free tropospheric aerosol at the Puy de Dôme (France) in winter. J. Geophys. Res. 108, 2002JD002747. https://doi.org/10.1029/2002JD002747

Tröstl, J., Herrmann, E., Frege, C., Bianchi, F., Molteni, U., Bukowiecki, N., Hoyle, C.R., Steinbacher, M., Weingartner, E., Dommen, J., Gysel, M., Baltensperger, U., 2016. Contribution of new particle formation to the total aerosol concentration at the high-altitude site Jungfraujoch (3580 m asl, Switzerland). JGR Atmospheres 121. https://doi.org/10.1002/2015JD024637

Vollmer, M.K., Steinbacher, M., Leuenberger, M.C., Emmenegger, L., 2020. The new 2020 air sampling inlet system at Jungfraujoch. https://www.hfsjg.ch/reports/2020/pdf/103_Empa_Vollmer_cf_mkv_neu.pdf

Vullo, E.L., Furlani, F., Arduini, J., Giostra, U., Cristofanelli, P., Williams, M.L., Maione, M., 2016. Non-Methane Volatile Organic Compounds in the Background Atmospheres of a Southern European Mountain Site (Mt. Cimone, Italy): Annual and Seasonal Variability. Aerosol Air Qual. Res. 16, 581–592. https://doi.org/10.4209/aaqr.2015.05.0364

Warburton, T., Lewis, A.C., Hopkins, J.R., Andrews, S.J., Yeoman, A.M., Owen, N., Jordan, C., Adamson, G., Xia, B., 2025. An assessment of VOC emissions and human strength perception of liquid electric fragrance diffusers. Environ. Sci.: Adv. 4, 739–752. https://doi.org/10.1039/D4VA00388H

Weingartner, E., Nyeki, S., Baltensperger, U., 1999. Seasonal and diurnal variation of aerosol size distributions ($10< D <750$ nm) at a high-alpine site (Jungfraujoch 3580 m asl). J. Geophys. Res. 104, 26809–26820. https://doi.org/10.1029/1999JD900170

Weng, J., Hao, Y., Brem, B.T., Cui, T., Khare, P., Dada, L., Daellenbach, K.R., Darfeuil, S., Uzu, G., Jaffrezo, J.-L., Steinbacher, M., Reimann, S., Gkraikou, T., Oikonomou, K., Sciare, J., Collaud Coen, M., Mohr, C., Prévôt, A.S.H., Gysel-Beer, M., El Haddad, I., Winiger, P., 2026. A Decadal-Scale Perspective on PM_{10} Composition and its Variability Drivers at the Alpine High-Altitude Research Station Jungfraujoch. https://doi.org/10.5194/egusphere-2026-3660

Whittlestone, S., Zahorowski, W., 1998. Baseline radon detectors for shipboard use: Development and deployment in the First Aerosol Characterization Experiment (ACE 1). J. Geophys. Res. 103, 16743–16751. https://doi.org/10.1029/98JD00687

Wiedensohler, A., Birmili, W., Nowak, A., Sonntag, A., Weinhold, K., Merkel, M., Wehner, B., Tuch, T., Pfeifer, S., Fiebig, M., Fjäraa, A.M., Asmi, E., Sellegri, K., Depuy, R., Venzac, H., Villani, P., Laj, P., Aalto, P., Ogren, J.A., Swietlicki, E., Williams, P., Roldin, P., Quincey, P., Hüglin, C., Fierz-Schmidhauser, R., Gysel, M., Weingartner, E., Riccobono, F., Santos, S., Grüning, C., Faloon, K., Beddows, D., Harrison, R., Monahan, C., Jennings, S.G., O'Dowd, C.D., Marinoni, A., Horn, H.-G., Keck, L., Jiang, J., Scheckman, J., McMurry, P.H., Deng, Z., Zhao, C.S., Moerman, M., Henzing, B., De Leeuw, G., Löschau, G., Bastian, S., 2012. Mobility particle size spectrometers: harmonization of technical standards and data structure to facilitate high quality long-term observations of atmospheric particle number size distributions. Atmos. Meas. Tech. 5, 657–685. https://doi.org/10.5194/amt-5-657-2012

Wu, F., Sun, J., Wang, Y., Liu, Z., 2025. Sources and Reactivity of Ambient VOCs on the Tibetan Plateau: Insights from a Multi-Site Campaign (2012–2014) for Assessing Decadal Change. Atmosphere 16, 1148. https://doi.org/10.3390/atmos16101148

Yang, M., Fleming, Z.L., 2019. Estimation of atmospheric total organic carbon (TOC) – paving the path towards carbon budget closure. Atmos. Chem. Phys. 19, 459–471. https://doi.org/10.5194/acp-19-459-2019

Yokelson, R.J., Crounse, J.D., DeCarlo, P.F., Karl, T., Urbanski, S., Atlas, E., Campos, T., Shinozuka, Y., Kapustin, V., Clarke, A.D., Weinheimer, A., Knapp, D.J., Montzka, D.D., Holloway, J., Weibring, P., Flocke, F., Zheng, W., Toohey, D., Wennberg, P.O., Wiedinmyer, C., Mauldin, L., Fried, A., Richter, D., Walega, J., Jimenez, J.L., Adachi, K., Buseck, P.R., Hall, S.R., Shetter, R., 2009. Emissions from biomass burning in the Yucatan. Atmospheric Chemistry and Physics 9, 5785–5812. https://doi.org/10.5194/acp-9-5785-2009

https://doi.org/10.5194/egusphere-2026-6814
Preprint. Discussion started: 12 November 2026
© Author(s) 2026. CC BY 4.0 License.

Yu, L., Smith, J., Laskin, A., George, K.M., Anastasio, C., Laskin, J., Dillner, A.M., Zhang, Q., 2016. Molecular transformations of phenolic SOA during photochemical aging in the aqueous phase: competition among oligomerization, functionalization, and fragmentation. Atmos. Chem. Phys. 16, 4511–4527. https://doi.org/10.5194/acp-16-4511-2016

Zanatta, M., Gysel, M., Bukowiecki, N., Müller, T., Weingartner, E., Areskoug, H., Fiebig, M., Yttri, K.E., Mihalopoulos, N., Kouvarakis, G., Beddows, D., Harrison, R.M., Cavalli, F., Putaud, J.P., Spindler, G., Wiedensohler, A., Alastuey, A., Pandolfi, M., Sellegri, K., Swietlicki, E., Jaffrezo, J.L., Baltensperger, U., Laj, P., 2016. A European aerosol phenomenology-5: Climatology of black carbon optical properties at 9 regional background sites across Europe. Atmospheric Environment 145, 346–364. https://doi.org/10.1016/j.atmosenv.2016.09.035

Zhou, S., Collier, S., Jaffe, D.A., Briggs, N.L., Hee, J., Sedlacek Iii, A.J., Kleinman, L., Onasch, T.B., Zhang, Q., 2017. Regional influence of wildfires on aerosol chemistry in the western US and insights into atmospheric aging of biomass burning organic aerosol. Atmos. Chem. Phys. 17, 2477–2493. https://doi.org/10.5194/acp-17-2477-2017